Pulse Sequences for Manipulating the Spin States of Molecular Radical-Pair-based Electron Spin Qubit Systems for Quantum Information Applications

Gediminas J. Pazera,¹ Matthew D. Krzyaniak,² and Michael R. Wasielewski²

²⁾Department of Chemistry and Center for Molecular Quantum Transduction, and Institute for Sustainability and Energy at Northwestern, Northwestern University, Evanston, Illinois 60208-3113, USA

(Dated: April 26, 2023)

¹⁾Department of Chemistry, University of Oxford, Physical and Theoretical Chemistry Laboratory, Oxford OX1 3QZ, UK.

I. ABSTRACT

Molecular qubits are an emerging platform in quantum information science (QIS) due to the unmatched structural control that chemical design and synthesis provide compared to other leading leading qubit technologies. This theoretical study investigates pulse sequence protocols for spin-correlated radical pairs (SCRPs), which are important molecular spin qubit pair (SQP) candidates. Here, we introduce improved microwave pulse protocols for enhancing the execution times of quantum logic gates based on SQPs. Significantly, this study demonstrates that the proposed pulse sequences effectively remove certain contributions from nuclear spin effects on spin dynamics, which are a common source of decoherence. Additionally, we have analyzed the factors that control the fidelity of the SQP spin state following application of the CNOT gate. It was found that higher magnetic fields introduce a high frequency oscillation in the fidelity. Thereupon, it is suggested that further research should be geared towards executing quantum gates at lower magnetic field values. In addition, an absolute bound of the fidelity outcome due to decoherence is determined, which clearly identifies the important factors that control gate execution. Finally, examples of the application of these pulse sequences to SQPs are described.

II. INTRODUCTION

There is a growing interest in molecular qubit systems comprising electron and nuclear spins for quantum information science (QIS) and quantum computing (QC). It stems from the extensive control over the qubit nature that chemical synthesis allows, providing the ability to fine-tune qubit properties and spatially position individual molecular qubits via covalent and non-covalent assemblies that may be used for quantum sensing (QS) or for preparing multi-qubit arrays.¹ Additionally, there are already a number of candidates for molecular qubits, such as photogenerated radical-pairs in donor-bridge-acceptor systems, ^{2,3} photogenerated radical pairs in triradical Pt complexes, ⁴ photoisomerization-induced spin-charge Co complexes, ⁵ and a recent example of a successful quantum teleportation experiment that utilized Electron Paramagnetic Resonance (EPR) for detection. ³ Besides the universal issue of coherence times and detection, alongside the experimental execution of quantum logic gates, further challenges need to be addressed. These challenges include a

full description of the dynamical properties of spin systems via computational or experimental techniques, coupling to external fields, electron-nuclear hyperfine interactions, spin-orbit coupling, magnetic spin exchange, and their effect on controlling the spin states. Furthermore, there is the matter of understanding environmental contributions to decoherence and how these effects impact molecular qubits. Addressing all of these issues would greatly accelerate the utilization of molecular systems in QIS and QS and provide a toolbox for designing new experiments and applications, which are only at the beginning stages of this emerging second quantum revolution.⁶

In Quantum Information Processing, there are several spin-based platforms outside molecular spin systems, such as impurities in semiconductors and quantum dots. Examples of impurities in semiconductors include coloured centres in diamond, such as nitrogen-vacancy, (NV), 7-10 and silicon-vacancy, (SV) centres, 11,12 and Phosphorus donor qubits in Silicon. 13,14 Much research has been conducted on these systems, which have several desirable characteristics, such as extended coherence times and optical addressability, and have been applied to sensing applications. However, they have encountered engineering and production obstacles. These materials have impurities that are difficult to manage, and spatial placement of defects, scalability to multiple qubits, and coupling of a large number of qubits are all difficult. In addition, Silicon 15-17 and germanium 18-20 quantum dots have been prominent QIP platforms. These are potential platforms with high fidelity rates, but similar to semiconductor impurities, they present fabrication and control issues. In addition to a high sensitivity to ambient and charge noise, which can reduce coherence times. This article is limited to molecular spin systems, which have been on the rise due to the ability of chemical synthesis to precisely control atomic placements.

Photogenerated SCRPs in donor-bridge-acceptor (D-B-A) molecules are one class of molecular qubit candidates that shows great promise. Their advantages can be readily demonstrated by considering the widely researched preparation, photophysics and spin dynamics of SCRPs, which are illustrated in Figure 1.^{21–25} In these systems, selective photoexcitation of D, B, or A produces an excited singlet state that undergoes rapid charge separation to produce a SCRP in an initial singlet spin state. This SCRP can be considered a spin qubit pair (SQP) and has been shown to satisfy a number of the DiVincenzo criteria.²⁶ The SCRPs are generated in a well-defined initial state, the systems are well-characterised, potentially scalable, and have been shown to have long coherence times, around 2 μs at rela-

tively high temperatures of 80 K.² SCRP coherence times can also be increased by reducing the electron-nuclear hyperfine interactions in each radical using deuteration and working in a nuclear spin free solvent, in addition to removing rapidly moving nuclear spins, such as the hydrogen atoms in methyl groups. Finally, a universal "set" of quantum logic gates exists, with initial attempts at implementation having been shown,^{2,27} and there is evidence of a qubit-specific measurement capability based on quantum state tomography;² however, further research needs to be done.

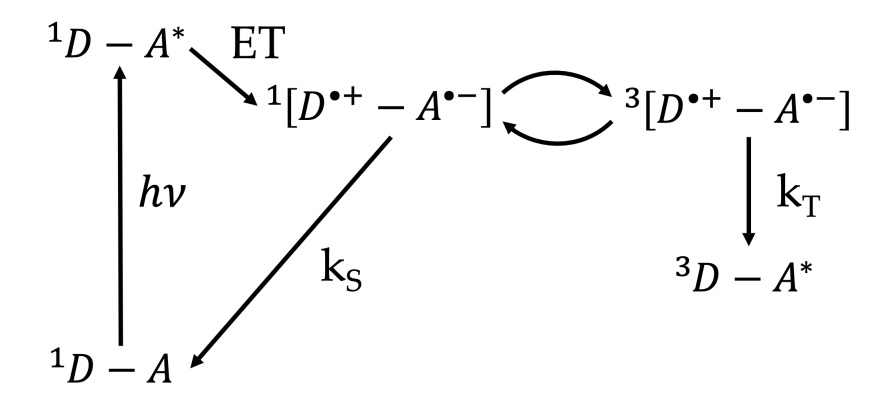


Figure 1: Scheme of a typical spin selective charge recombination reaction in donor-acceptor (D-A) molecules. After initial light excitation and electron transfer reactions, a SCRP in a singlet state is produced, $[D^{\bullet+} - A^{\bullet-}]^1$. The singlet state can interconvert to the triplet state $[D^{\bullet+} - A^{\bullet-}]^3$ via hyperfine interactions of each of the spins. Both of these states relax to the ground state via different pathways. The singlet state relaxes to the ground state via the singlet pathway with recombination constant k_S , and the triplet state recombines to a triplet product via the triplet pathway with recombination constant k_T .

With respect to QIS, there are a few general criteria for a good SCRP system: First, the SCRP should have intermediate electron spin–spin coupling because this value will ultimately determine the speed at which a gate can be executed. Second, the SCRP should have long coherence times, T_2 to ensure that a sufficient number of gate operations can be made to be useful; Third, the SCRP should be capable of being oriented in a well-defined, controllable position to avoid overlapping transitions and to enable proper readout and control of the spin system. For example, oriented single crystals would be ideal in this regard.

In this article we will explore how quantum logic gates can be implemented in a SCRP

system. We will propose improved pulse sequences for most common two-qubit quantum logic gates in SCRPs and introduce ways to correct for different noise sources in the experimental application of these quantum logic gates. Furthermore, we will give a full dynamical description of how the fidelity of the SQP spin system following CNOT gate application will vary with different parameters in the experiment and give evidence for the advantages of performing these experiments at lower magnetic fields. Lastly, a universal bound on the fidelity value of a CNOT gate operation will be given when T_2 relaxation effects are incorporated, providing an understanding of how decoherence affects SQPs.

III. THEORY

A. Spin Hamiltonian

The spin dynamics of an arbitrary SCRP in a fixed orientation are governed by its spin Hamiltonian, which includes the anisotropic electron Zeeman interaction, electron–nuclear hyperfine interaction, electron–electron dipolar interaction and electron exchange interaction.^{28–30} If the applied magnetic field is larger than other interactions in the system, then a secular approximation can be employed which simplifies the Hamiltonian to:^{27,30–32}

$$\hat{H} = \hat{H}_{12} + \hat{H}_{hyp} \tag{1}$$

where,

$$\hat{H}_{12} = g_1 \mu_B |\mathbf{B}| \, \hat{S}_{1z} + g_2 \mu_B |\mathbf{B}| \, \hat{S}_{2z} + J \hat{\mathbf{S}}_1^T \hat{\mathbf{S}}_2 + \frac{1}{2} \mathcal{D} \left(3 \hat{S}_{1z} \hat{S}_{2z} - \hat{\mathbf{S}}_1^T \hat{\mathbf{S}}_2 \right)$$

$$= \omega_1 \hat{S}_{1z} + \omega_2 \hat{S}_{2z} + \mathcal{D}_1 \hat{S}_{1z} \hat{S}_{2z} + \mathcal{D}_2 \left(\hat{S}_{1x} \hat{S}_{2x} + \hat{S}_{1y} \hat{S}_{2y} \right)$$
(2)

$$\hat{H}_{Hyp} = \hat{S}_{1z} \left(\sum_{k=1}^{N_1} \left(A_{1k} \hat{I}_{1k,z} + B_{1k} \hat{I}_{1k,x} \right) \right) + \hat{S}_{2z} \left(\sum_{p=1}^{N_2} \left(A_{2p} \hat{I}_{2p,z} + B_{2p} \hat{I}_{2p,x} \right) \right)$$
(3)

and

$$\mathcal{D} = D \left(\cos^2(\theta) - \frac{1}{3} \right)$$

$$\mathcal{D}_1 = \mathcal{D} + J$$

$$\mathcal{D}_2 = -\frac{\mathcal{D}}{2} + J$$
(4)

Here **B** is the applied magnetic field, $\hat{\mathbf{S}}_i$ and $\hat{\mathbf{I}}_{ik}$ are electron and nuclear spin operators, respectively, N_i is the number of nuclear spins coupled to radical i, θ is the angle between the applied magnetic eld and the dipolar axis, J is the electron exchange interaction constant, D is the strength of the dipolar interaction, μ_B is Bohr magneton, and g_i is the g tensor. With the additional simplification, ω_i is the Zeeman frequency of radical i under the applied magnetic field of strength $|\mathbf{B}|$.

Eigenvectors and eigenvalues for \hat{H}_{12} are:^{33,34}

$$|1\rangle = |T_{+}\rangle; |2\rangle = \cos \xi |S\rangle + \sin \xi |T_{0}\rangle$$

$$|3\rangle = -\sin \xi |S\rangle + \cos \xi |T_{0}\rangle; |4\rangle = |T_{-}\rangle$$
(5)

$$\lambda_1 = \frac{\Omega}{2} + \frac{\mathcal{D}_1}{4}; \ \lambda_2 = -\frac{1}{2}\Theta - \frac{\mathcal{D}_1}{4}$$

$$\lambda_3 = \frac{1}{2}\Theta - \frac{\mathcal{D}_1}{4}; \ \lambda_4 = -\frac{\Omega}{2} + \frac{\mathcal{D}_1}{4}$$
(6)

where,

$$\tan\left(2\xi\right) = \frac{-\Delta\omega}{\frac{2}{3}\mathcal{D}_1 + \frac{1}{3}\mathcal{D}_2}\tag{7}$$

$$\Delta\omega = \omega_2 - \omega_1; \ \Omega = \omega_1 + \omega_2; \Theta = \sqrt{\Delta\omega^2 + \mathcal{D}_2^2}$$
 (8)

The electron spin - electron spin Hamiltonian, \hat{H}_{12} , can be further reduced at very high magnetic fields if the difference between Zeeman energies is much larger than spin interactions, i.e. $|\omega_2 - \omega_1| \gg \mathcal{D}_1$:

$$\hat{H}_{12} = \omega_1 \hat{S}_{1z} + \omega_2 \hat{S}_{2z} + \mathcal{D}_1 \hat{S}_{1z} \hat{S}_{2z} \tag{9}$$

In this study, only the \hat{H}_{12} term of the full \hat{H} will be used for the design of the pulse sequences and the influence of \hat{H}_{hyp} on dynamics will be discussed separately. Furthermore, the three main cases of high field \hat{H} will be discussed during the design of pulse sequences:

1. \hat{H} with only $\hat{S}_{1z}\hat{S}_{2z}$ interaction:

$$\hat{H}_1 = \mathcal{D}_1 \hat{S}_{1z} \hat{S}_{2z} \tag{10}$$

2. High field \hat{H} with $|\omega_2 - \omega_1| \gg D_1$:

$$\hat{H}_2 = \omega_1 \hat{S}_{1z} + \omega_2 \hat{S}_{2z} + \mathcal{D}_1 \hat{S}_{1z} \hat{S}_{2z} \tag{11}$$

3. High field \hat{H} :

$$\hat{H}_3 = \omega_1 \hat{S}_{1z} + \omega_2 \hat{S}_{2z} + \mathcal{D}_1 \hat{S}_{1z} \hat{S}_{2z} + \mathcal{D}_2 \left(\hat{S}_{1x} \hat{S}_{2x} + \hat{S}_{1y} \hat{S}_{2y} \right)$$
(12)

B. Idempotent operators

A neat and simple tool to derive an analytical form of any two spin pulse sequence, first introduced by Price et al.,³⁵ involves the use of primitive idempotent operators, E_{\pm} , that satisfy the following properties:

$$E_{+} + E_{-} = 1, \ E_{\pm}^{2} = E_{\pm}, \ E_{+}E_{-} = 0$$
 (13)

Important idempotent operators for electron spins are:

$$E_{\pm}^{i} = \frac{1}{2}\mathbb{I} \pm \hat{S}_{iz}, \ E_{\pm}^{i,j} = \frac{1}{2}\mathbb{I} \pm 2\hat{S}_{iz}\hat{S}_{jz}$$
 (14)

Thus, an arbitrary density matrix,

$$\hat{U} = \begin{pmatrix} u_{11} & u_{12} & u_{13} & u_{14} \\ u_{21} & u_{22} & u_{23} & u_{24} \\ u_{31} & u_{32} & u_{33} & u_{34} \\ u_{41} & u_{42} & u_{43} & u_{44} \end{pmatrix}$$
(15)

can be decomposed using idempotent operators:²⁷

$$\hat{U} = u_{11}E_{+}^{1}E_{+}^{2} + 2u_{12}\hat{S}_{2x}E_{+}^{1}E_{-}^{2} + 2u_{13}\hat{S}_{1x}E_{-}^{1}E_{+}^{2} + 4u_{14}\hat{S}_{1x}\hat{S}_{2x}E_{-}^{1}E_{-}^{2}
+ 2u_{21}\hat{S}_{2x}E_{+}^{1}E_{+}^{2} + u_{22}E_{+}^{1}E_{-}^{2} + 4u_{23}\hat{S}_{1x}\hat{S}_{2x}E_{-}^{1}E_{+}^{2} + 2u_{24}\hat{S}_{1x}E_{-}^{1}E_{-}^{2}
+ 2u_{31}\hat{S}_{1x}E_{+}^{1}E_{+}^{2} + 4u_{32}\hat{S}_{1x}\hat{S}_{2x}E_{+}^{1}E_{-}^{2} + u_{33}E_{-}^{1}E_{+}^{2} + 2u_{34}\hat{S}_{2x}E_{-}^{1}E_{-}^{2}
+ 4u_{41}\hat{S}_{1x}\hat{S}_{2x}E_{+}^{1}E_{+}^{2} + 2u_{42}\hat{S}_{1x}E_{+}^{1}E_{-}^{2} + 2u_{43}\hat{S}_{2x}E_{-}^{1}E_{+}^{2} + u_{44}E_{-}^{1}E_{-}^{2}$$
(16)

This provides a straightforward way to find a decomposition for any two-spin quantum gate. An important property for idempotent operators used throughout this work is:

$$e^{AE_{\pm}} = e^A E_{\pm} + E_{\mp}$$
, given that $[A, E_{\pm}] = 0$ (17)

Lastly, an important property for the exponential of an arbitrary Pauli spin matrix \hat{S}_k is:

$$e^{i\theta\hat{S}_k} = \cos\left(\frac{\theta}{2}\right)\mathbb{I} + i2\hat{S}_k\sin\left(\frac{\theta}{2}\right)$$
 (18)

C. Fidelity

The general measure of closeness between two quantum states is called the fidelity and it can be computed with knowledge of their density matrices $\hat{\rho}$ and $\hat{\sigma}$ using the following equation:³⁶

$$\mathcal{F}(\hat{\rho}, \hat{\sigma}) = \left(\text{Tr} \sqrt{\hat{\rho}^{1/2} \hat{\sigma} \hat{\rho}^{1/2}} \right)^2 \tag{19}$$

Here $\hat{\rho}$ is taken to be the ideal density matrix state and $\hat{\sigma}$ is the experimentally measured density matrix, for instance, determined by quantum state tomography.²

In the case of an initial pure state $\hat{\rho}(0) = |\Psi\rangle\langle\Psi|$ and $\hat{\rho} = \hat{U}_{ideal}\hat{\rho}(0)\hat{U}_{ideal}^{\dagger}$, where \hat{U}_{ideal} is trace preserving, the fidelity measure simplifies to:

$$\mathcal{F} = \langle \Psi | \, \hat{U}_{ideal}^{\dagger} \hat{\sigma} \hat{U}_{ideal} \, | \Psi \rangle \tag{20}$$

Given that $\hat{\rho}^2 = \hat{\rho}$. Here \hat{U}_{ideal} is the ideal case propagation matrix. If we can easily decompose $\hat{\sigma} = \hat{U}_{spin} |\Psi\rangle \langle\Psi| \hat{U}_{spin}^{\dagger}$, then the fidelity measure will be:

$$\mathcal{F} = \left| \langle \Psi | \, \hat{U}_{ideal}^{\dagger} \hat{U}_{spin} \, | \Psi \rangle \right|^{2} \tag{21}$$

where \hat{U}_{spin} is resultant propagator under arbitrary spin evolution and rotation pulses.

For instance, if the system has two electron spins that are initialized in a singlet state, and the ideal gate is a CNOT gate, then the fidelity will be:

$$\mathcal{F} = \left| \langle S | \, \hat{U}_{CNOT}^{\dagger} \hat{U}_{spin} \, | S \rangle \right|^{2} \tag{22}$$

IV. PULSE SEQUENCES FOR TWO QUBIT GATES

The general algorithm for deriving a pulse sequence is as follows: First, expand the target propagator using idempotent operators. Second, derive a pulse sequence for a Hamiltonian that only includes the electron spin - electron spin interaction. Third, apply correction terms to the pulse sequence to account for other Hamiltonian terms.^{27,35}

In this section, the procedure for generating a pulse sequence will be demonstrated by finding the Controlled-NOT (CNOT) gate pulse sequence for a SCRP system. Considering that the pulse sequence is derived for a Hamiltonian without Zeeman and hyperfine interactions, a correction term will be proposed, which will also alleviate the influence of hyperfine interactions on the fidelity measure. In addition to the CNOT gate, the pulse sequence for other generally used two qubit gates will be introduced. Finally, a simplification for a CNOT gate for a SCRP starting in a singlet state will be demonstrated that will significantly reduce the number of pulses needed to execute the gate.

A. Pulse sequence for a CNOT gate

The CNOT gate is one of the fundamental two qubit quantum logic gates that when combined with several single qubit gates forms a complete set of quantum logic gates from which any arbitrary unitary transformation can be derived.²⁶ The propagator matrix takes the form:

$$\hat{U}_{CNOT} = \begin{pmatrix} 1 & 0 & 0 & 0 \\ 0 & 1 & 0 & 0 \\ 0 & 0 & 0 & 1 \\ 0 & 0 & 1 & 0 \end{pmatrix}$$

$$(23)$$

Its main action is the inversion of $|\beta\alpha\rangle$ and $|\beta\beta\rangle$ populations in a two qubit system that manifests from the state of the first (called the control) qubit. If the first qubit is in $|\beta\rangle$ state then the state of the second (called the target) qubit is flipped. The unitary matrix formed with the expansion in Eq. 16 for this gate is:

$$\hat{U}_{CNOT} = E_{\perp}^{1} + 2\hat{S}_{2x}E_{\perp}^{1} \tag{24}$$

Given that a pulse sequence is essentially a set of multiplied exponential matrices it becomes possible to find a binomial multiplication for the expansion that will transform it into an experimentally feasible pulse sequence:

$$\hat{U}_{CNOT} = E_{+}^{1} + 2\hat{S}_{2x}E_{-}^{1}$$

$$= E_{+}^{1} + i(-i)2\hat{S}_{2x}E_{-}^{1}$$

$$= \left(-i2\hat{S}_{2x}E_{-}^{1} + E_{+}^{1}\right)\left(iE_{-}^{1} + E_{+}^{1}\right)$$
(25)

By applying Eq. 17 and noting that $e^{i\pi/2} = i$ and $e^{-i\pi \hat{S}_{2x}} = -2i\hat{S}_{2x}$ according to Eq. 18, we find:

$$\hat{U}_{CNOT} = e^{-i\pi \hat{S}_{2x} E_{-}^{1}} e^{i\frac{\pi}{2} E_{-}^{1}} \tag{26}$$

Using the definitions in Eq. 14, this is expanded as:

$$\hat{U}_{CNOT} = e^{i\frac{\pi}{4}} e^{-i\frac{\pi}{2}\hat{S}_{2x}} e^{-i\frac{\pi}{2}\hat{S}_{1z}} e^{i\pi\hat{S}_{1z}\hat{S}_{2x}}$$
(27)

Due to the nature of the experimental setup and the spin Hamiltonian, the \hat{S}_{1z} and $\hat{S}_{1z}\hat{S}_{2z}$ terms cannot be directly generated in the experiment. These exponential terms have to be decomposed into a form more suited for experimental implementation. There are a large number of ways to decompose these terms; in addition, the terms in Eq. 27 commute with each other resulting in many different pulse sequences that can achieve the same unitary transformation. One possible solution, with a particularly clean structure, is as follows:

$$e^{-i\frac{\pi}{2}\hat{S}_{1z}} = e^{i\frac{\pi}{2}\hat{S}_{1x}}e^{i\frac{\pi}{2}\hat{S}_{1y}}e^{-i\frac{\pi}{2}\hat{S}_{1x}} \tag{28}$$

$$e^{i\pi\hat{S}_{1z}\hat{S}_{2x}} = e^{-i\frac{\pi}{2}\hat{S}_{2y}}e^{i\pi\hat{S}_{1z}\hat{S}_{2z}}e^{i\frac{\pi}{2}\hat{S}_{2y}}$$
(29)

Substituting Eq. 28 and 29 into Eq. 27 yields:

$$\hat{U}_{CNOT} = e^{i\frac{\pi}{4}} e^{-i\frac{\pi}{2}\hat{S}_{2y}} e^{i\pi\hat{S}_{1z}\hat{S}_{2z}} e^{i\frac{\pi}{2}\hat{S}_{1x}} e^{i\frac{\pi}{2}(\hat{S}_{1y} + \hat{S}_{2y})} e^{-i\frac{\pi}{2}(\hat{S}_{1x} + \hat{S}_{2x})}$$
(30)

For the reduced high field Hamiltonian in Eq. 10, the rotation term, $\hat{S}_{1z}\hat{S}_{2z}$, can be treated as a time propagation under the spin Hamiltonian:

$$e^{-i\hat{H}_{1}\tau} = e^{i\pi\hat{S}_{1z}\hat{S}_{2z}}$$

$$-i\hat{H}_{1}\tau = i\pi\hat{S}_{1z}\hat{S}_{2z}$$

$$-i\mathcal{D}_{1}\tau\hat{S}_{1z}\hat{S}_{2z} = i\pi\hat{S}_{1z}\hat{S}_{2z}$$

$$\tau = -\frac{\pi}{\mathcal{D}_{1}} = \frac{\pi}{|\mathcal{D}_{1}|}$$
(31)

Note that $\mathcal{D}_1 < 0$. The pulse sequence for the CNOT gate (read from left to right, this notation will be used throughout this paper) is:

$$90^{\circ}_{1x+2x}, \ 90^{\circ}_{-(1y+2y)}, \ 90^{\circ}_{-1x}, \ \frac{\pi}{|\mathcal{D}_1|}, \ 90^{\circ}_{2y}$$
 (32)

Here the degrees show the magnitude of spin selective or non-selective rotations and the subscripted index identifies each electron spin and its phase. The non-degree term represents the propagation time required for the system.

1. The sign of \mathcal{D}_1

The reported sequences in Ref. 27 have this form for the spin evolution time:

$$\tau = \frac{\pi}{\mathcal{D}_1} \tag{33}$$

Since, as defined in Eq. 2, \mathcal{D}_1 is a negative quantity for radical pairs, the reported SWAP and CNOT gate sequences for electron spins are not appropriate since $\pi/\mathcal{D}_1 \neq \pi/|\mathcal{D}_1|$. If $\tau = \pi/\mathcal{D}_1$, the actual CNOT pulse sequence suggested by Ref. 27, which was recently employed in Ref. 37 takes the form (with adjusted phase):

$$\hat{U}_{CNOT} = \begin{pmatrix} 0 & -1 & 0 & 0 \\ -1 & 0 & 0 & 0 \\ 0 & 0 & 1 & 0 \\ 0 & 0 & 0 & 1 \end{pmatrix}$$

$$(34)$$

Care must be taken when using pulse sequences to be sure the right sequence is used for the appropriate case.

B. Corrections for Zeeman Interactions

The derived pulse sequence in Eq.32, namely the $\hat{S}_{1z}\hat{S}_{2z}$ evolution, breaks down when including the electron Zeeman terms such as in Eqs. 11, 12. The general way to correct this is to split the spin evolution term into two equal parts and apply an additional pulse sequence, which will selectively rotate only the \hat{S}_{iz} terms and cancel the other Zeeman terms.²⁷ Under the influence of Eq. 11 this method yields:

$$e^{i\pi\hat{S}_{1z}\hat{S}_{2z}} = e^{-i\hat{H}_{2}\frac{\tau}{2}}e^{-i\pi\left(\hat{S}_{1x}+\hat{S}_{2x}\right)}e^{-i\hat{H}_{2}\frac{\tau}{2}}e^{i\pi\left(\hat{S}_{1x}+\hat{S}_{2x}\right)}$$

$$= e^{-i\left(\omega_{1}\hat{S}_{1z}+\omega_{2}\hat{S}_{2z}+\mathcal{D}_{1}\hat{S}_{1z}\hat{S}_{2z}\right)\frac{\tau}{2}}e^{-i\pi\left(\hat{S}_{1x}+\hat{S}_{2x}\right)}e^{-i\left(\omega_{1}\hat{S}_{1z}+\omega_{2}\hat{S}_{2z}+\mathcal{D}_{1}\hat{S}_{1z}\hat{S}_{2z}\right)\frac{\tau}{2}}e^{i\pi\left(\hat{S}_{1x}+\hat{S}_{2x}\right)}$$

$$= e^{-i\left(\omega_{1}\hat{S}_{1z}+\omega_{2}\hat{S}_{2z}+\mathcal{D}_{1}\hat{S}_{1z}\hat{S}_{2z}\right)\frac{\tau}{2}}e^{-i\left(-\omega_{1}\hat{S}_{1z}-\omega_{2}\hat{S}_{2z}+\mathcal{D}_{1}\hat{S}_{1z}\hat{S}_{2z}\right)\frac{\tau}{2}}$$

$$= e^{-i\mathcal{D}_{1}\hat{S}_{1z}\hat{S}_{2z}\tau}$$

$$(35)$$

Hence, for each pulse sequence evolving under Eq. 11, the propagation time τ is replaced by:

$$\tau \to 180^{\circ}_{-(1x+2x)}, \ \frac{\tau}{2}, \ 180^{\circ}_{1x+2x}, \ \frac{\tau}{2}$$
 (36)

For the time evolution under Eq. 12 a correction sequence that divides the spin evolution time into four parts was suggested in Ref. 27. We note that the same result can be achieved with fewer dissections and pulse sequences:

$$e^{i\pi\hat{S}_{1z}\hat{S}_{2z}} = e^{-i\hat{H}_{3}\frac{\tau}{2}}e^{-i\pi\hat{S}_{1x}}e^{-i\pi\hat{S}_{2y}}e^{-i\hat{H}_{3}\frac{\tau}{2}}e^{i\pi\hat{S}_{1x}}e^{i\pi\hat{S}_{2y}}$$

$$= e^{-i\hat{H}_{3}\frac{\tau}{2}}e^{-i\left(-\omega_{1}\hat{S}_{1z}-\omega_{2}\hat{S}_{2z}+\mathcal{D}_{1}\hat{S}_{1z}\hat{S}_{2z}-\mathcal{D}_{2}\left(\hat{S}_{1x}\hat{S}_{2x}+\hat{S}_{1y}\hat{S}_{2y}\right)\right)\frac{\tau}{2}}$$

$$= e^{-i\hat{D}_{1}\hat{S}_{1z}\hat{S}_{2z}\tau}$$
(37)

The two exponential terms can be added because the expressions commute. For every pulse sequence that evolves under Eq. 12 the propagation time τ is replaced by:

$$\tau \to 180^{\circ}_{-1x}, 180^{\circ}_{-2y}, \ \frac{\tau}{2}, \ 180^{\circ}_{1x}, \ 180^{\circ}_{2y}, \ \frac{\tau}{2}$$
 (38)

C. Hyperfine Interaction Effects

The hyperfine interaction, which arises from nuclear spins, is typically non-negligible in SCRP systems and is often of a similar order of magnitude to the D coupling. Nuclear spins significantly influence the experimental setting by altering the initial pulse response, affecting readout through modulation effects, and introducing additional sources of noise. Whenever possible, these effects should be mitigated through chemical synthesis or isotopic labelling, as well as by creating an environment that minimizes spin decoherence, such as employing specific solvents and maintaining low temperatures. Notably, the correction factors introduced earlier can also eliminate some contributions from hyperfine interaction terms, potentially enhancing the fidelity of the two Qubit gate in situations where nuclear spin effects cannot be mitigated.

When we add static hyperfine coupling effects to the correction sequence in Eq. 36. we find:

$$e^{i\pi\hat{S}_{1z}\hat{S}_{2z}} = e^{-i\hat{H}_{hyp,2}\frac{\tau}{2}}e^{-i\pi\left(\hat{S}_{1x}+\hat{S}_{2x}\right)}e^{-i\hat{H}_{hyp,2}\frac{\tau}{2}}e^{i\pi\left(\hat{S}_{1x}+\hat{S}_{2x}\right)}$$

$$= e^{-i\hat{H}_{hyp,2}\frac{\tau}{2}}e^{-i\hat{H}'_{hyp,2}\frac{\tau}{2}}$$
(39)

where,

$$\hat{H}_{hyp,2} = \hat{H}_2 + \hat{H}_{hyp} \tag{40}$$

$$\hat{H}_{hyp} = \hat{S}_{1z} \left(\sum_{k=1}^{N_1} \left(A_{1k} \hat{I}_{1k,z} + B_{1k} \hat{I}_{1k,x} \right) \right) + \hat{S}_{2z} \left(\sum_{p=1}^{N_2} \left(A_{2p} \hat{I}_{2p,z} + B_{2p} \hat{I}_{2p,x} \right) \right)$$
(41)

$$\hat{H}'_{hyp,2} = \hat{H}'_2 - \hat{H}_{hyp} \tag{42}$$

$$\hat{H}_{2}' = -\omega_{1}\hat{S}_{1z} - \omega_{2}\hat{S}_{2z} + \mathcal{D}_{1}\hat{S}_{1z}\hat{S}_{2z}$$

$$\tag{43}$$

Since $\left[\hat{H}_{hyp,2},\hat{H}'_{hyp,2}\right]=0$ (proof of which is shown in Appendix A):

$$e^{-i\hat{H}_{hyp,2}\frac{\tau}{2}}e^{-i\hat{H}'_{hyp,2}\frac{\tau}{2}} = e^{-i\left(\hat{H}_{hyp,2} + \hat{H}'_{hyp,2}\right)\frac{\tau}{2}} = e^{-i\mathcal{D}_1\hat{S}_{1z}\hat{S}_{2z}\tau} = e^{i\pi\hat{S}_{1z}\hat{S}_{2z}} \tag{44}$$

This shows that the overall performance in terms of fidelity of a pulse sequence for \hat{H}_2 will be unaffected by the static hyperfine interactions of the system.

An equivalent result can be seen for the correction sequence in Eq. 38 since $\left[\hat{H}_{hyp,3},\hat{H}'_{hyp,3}\right] = 0$ (proof in Appendix A), where

$$\hat{H}_{hyp,3} = \hat{H}_3 + \hat{H}_{hyp} \tag{45}$$

$$\hat{H}'_{hyp,3} = \hat{H}'_3 - \hat{H}_{hyp} \tag{46}$$

$$\hat{H}_{3}' = -\omega_{1}\hat{S}_{1z} - \omega_{2}\hat{S}_{2z} + \mathcal{D}_{1}\hat{S}_{1z}\hat{S}_{2z} - \mathcal{D}_{2}\left(\hat{S}_{1x}\hat{S}_{2x} + \hat{S}_{1y}\hat{S}_{2y}\right) \tag{47}$$

The result presented above assumes that nuclear Zeeman effects are negligible in the dynamics due to their small magnitude compared to the electron spin Zeeman effect. If these effects are included in the dynamics, the time-propagation sequence becomes:

$$e^{-i\pi\hat{S}_{1z}\hat{S}_{2z}} = e^{-i\mathcal{D}_1\hat{S}_{1z}\hat{S}_{2z}\tau}e^{-i\sum_{k=1}^{N_1}\omega_{1k}\hat{I}_{1k,z}\tau}e^{-i\sum_{p=1}^{N_2}\omega_{2p}\hat{I}_{2p,z}\tau}$$
(48)

Where ω_{ij} is gyromagnetic ratio of nuclei j coupled to electron spin i.

Although this effect will undoubtedly influence the spin dynamics for high magnetic fields, if the nuclear spin space-which is a commonly assumed to be in a fully mixed state-and the electron spin space are not coupled for the initial nuclear spin space then the nuclear Zeeman effect will not affect the fidelity measure because it does not evolve the electron spin states. However, it is likely to affect the experimental readout, which is not addressed in this article.

D. Proposed Pulse Sequences

The most common two qubit quantum logical gates are the CNOT, SWAP, Controlled-Z, and Controlled-Phase gates.³⁶ Their propagators and pulses sequences are depicted in Table I. The pulse sequences were derived with evolution under Eq. 10, but can easily be expanded

to account for Eqs. 11 and 12 as we have already demonstrated. All derivations are shown in Appendix B.

Operation	Propagator	Pulse Sequence
\hat{U}_{CNOT}	$ \begin{pmatrix} 1 & 0 & 0 & 0 \\ 0 & 1 & 0 & 0 \\ 0 & 0 & 0 & 1 \\ 0 & 0 & 1 & 0 \end{pmatrix} $	$90^{\circ}_{1x+2x}, \ 90^{\circ}_{-(1x+2x)}, \ 90^{\circ}_{-1x}, \ \frac{\pi}{ \mathcal{D}_1 }, \ 90^{\circ}_{2y}$
\hat{U}_{SWAP}	$\begin{pmatrix} 1 & 0 & 0 & 0 \\ 0 & 0 & 1 & 0 \\ 0 & 1 & 0 & 0 \\ 0 & 0 & 0 & 1 \end{pmatrix}$	$90^{\circ}_{1x+2x}, \frac{\pi}{ \mathcal{D}_1 }, 90^{\circ}_{-(1x+2x)}, 90^{\circ}_{1y+2y}, \frac{\pi}{ \mathcal{D}_1 } 90^{\circ}_{-(1y+2y)}, \frac{\pi}{ \mathcal{D}_1 }$
\hat{U}_{CZ}	$\begin{pmatrix} 1 & 0 & 0 & 0 \\ 0 & 1 & 0 & 0 \\ 0 & 0 & 1 & 0 \\ 0 & 0 & 0 & -1 \end{pmatrix}$	$90^{\circ}_{-1x}, \ 90^{\circ}_{1y+2y}, \ 90^{\circ}_{1x+2x}, \ 90^{\circ}_{-2y}, \ \frac{\pi}{ \mathcal{D}_1 }$
$\hat{U}_{CP}\left(\phi ight)$	$\begin{pmatrix} 1 & 0 & 0 & 0 \\ 0 & 1 & 0 & 0 \\ 0 & 0 & 1 & 0 \\ 0 & 0 & 0 & -1 \end{pmatrix}$ $\begin{pmatrix} 1 & 0 & 0 & 0 \\ 0 & 1 & 0 & 0 \\ 0 & 0 & 1 & 0 \\ 0 & 0 & 0 & e^{i\phi} \end{pmatrix}$	$90_{2x}^{\circ}, \ \left(\frac{\phi}{2}\right)_{-2y}^{\circ}, \ 90_{-2x}^{\circ}, \ 90_{-1y}^{\circ}, \ \left(\frac{\phi}{2}\right)_{-1x}^{\circ}, \ 90_{1y}^{\circ}, \ \frac{\phi}{ \mathcal{D}_1 }$

Table I: Pulse sequences for Controlled-NOT (CNOT), SWAP, Controlled-Z (CZ), and Controlled-Phase (CP) quantum logic gates for coupled electron spin systems. All of the pulse sequences were derived assuming \hat{H}_1 in Eq. 10, yet the pulse sequences can be extended with the proposed correction terms for other Hamiltonians. Pulse sequences are read from left to right.

E. Simplification of the CNOT Gate Pulse Sequence for an Initial Singlet State

The propagator for a CNOT gate according to Eq. 10 is:

$$\hat{U}_{CNOT} = e^{i\frac{\pi}{4}} e^{-i\frac{\pi}{2}\hat{S}_{2y}} e^{-i\hat{H}_{1}\tau} e^{i\frac{\pi}{2}\hat{S}_{1x}} e^{i\frac{\pi}{2}(\hat{S}_{1y} + \hat{S}_{2y})} e^{-i\frac{\pi}{2}(\hat{S}_{1x} + \hat{S}_{2x})}$$
(49)

Here $\tau = \pi/\mathcal{D}_1$. If the starting state is a pure singlet state, which is true in most cases for radical pair systems, and owing to the fact that applying \hat{U}_{CNOT} to an initial density matrix $\hat{\rho}(0)$ results in $\hat{\rho} = \hat{U}_{CNOT} \rho(\hat{0}) \hat{U}_{CNOT}^{\dagger}$, we note that the two non-selective pulses will cancel:

$$e^{i\frac{\pi}{2}(\hat{S}_{1y}+\hat{S}_{2y})}e^{-i\frac{\pi}{2}(\hat{S}_{1x}+\hat{S}_{2x})}\hat{\rho}(0)e^{i\frac{\pi}{2}(\hat{S}_{1x}+\hat{S}_{2x})}e^{-i\frac{\pi}{2}(\hat{S}_{1y}+\hat{S}_{2y})}=\hat{\rho}(0)$$
(50)

reducing the propagator for pure singlet initial state to:

$$\hat{U}_{CNOT} = e^{i\frac{\pi}{4}} e^{-i\frac{\pi}{2}\hat{S}_{2y}} e^{-i\hat{H}_{1}\tau} e^{i\frac{\pi}{2}\hat{S}_{1x}}$$
(51)

or to this pulse sequence:

$$90^{\circ}_{-1x}, \ \tau, \ 90^{\circ}_{2y}$$
 (52)

If the spin evolution is done according to Eq. 11 and correction in Eq. 36 is employed, the propagator is:

$$\hat{U}_{CNOT} = e^{i\frac{\pi}{4}} e^{-i\frac{\pi}{2}\hat{S}_{2y}} e^{-i\hat{H}_{2}\frac{\tau}{2}} e^{-i\pi(\hat{S}_{1x} + \hat{S}_{2x})} e^{-i\hat{H}_{2}\frac{\tau}{2}} e^{i\pi(\hat{S}_{1x} + \hat{S}_{2x})} e^{i\frac{\pi}{2}\hat{S}_{1x}}
= e^{i\frac{\pi}{4}} e^{-i\frac{\pi}{2}\hat{S}_{2y}} e^{-i\hat{H}_{2}\frac{\tau}{2}} e^{-i\pi(\hat{S}_{1x} + \hat{S}_{2x})} e^{-i\hat{H}_{2}\frac{\tau}{2}} e^{i\frac{\pi}{2}\hat{S}_{1x}} e^{i\pi(\hat{S}_{1x} + \hat{S}_{2x})}$$
(53)

We can do another simplification since:

$$e^{i\pi(\hat{S}_{1x}+\hat{S}_{2x})}\hat{\rho}(0)e^{-i\pi(\hat{S}_{1x}+\hat{S}_{2x})} = \hat{\rho}(0)$$
(54)

reducing the operator:

$$\hat{U}_{CNOT} = e^{i\frac{\pi}{4}} e^{-i\frac{\pi}{2}\hat{S}_{2y}} e^{-i\hat{H}_2\frac{\tau}{2}} e^{-i\pi(\hat{S}_{1x} + \hat{S}_{2x})} e^{-i\hat{H}_2\frac{\tau}{2}} e^{i\frac{\pi}{2}\hat{S}_{1x}}$$
(55)

yielding a simple three pulse sequence:

$$90^{\circ}_{-1x}, \ \tau_1, \ 180^{\circ}_{1x+2x}, \ \tau_2, \ 90^{\circ}_{2y}$$
 (56)

Here τ_1 and τ_2 are arbitrary spin evolution times and should be multiples of $\pi/(2\mathcal{D}_1)$.

Finally, evolution according to Eq. 12 provides the corrected sequence in Eq. 38:

$$\hat{U}_{CNOT} = e^{i\frac{\pi}{4}} e^{-i\frac{\pi}{2}\hat{S}_{2y}} e^{-i\hat{H}_{3}\frac{\tau}{2}} e^{-i\pi\hat{S}_{1x}} e^{-i\pi\hat{S}_{2y}} e^{-i\hat{H}_{3}\frac{\tau}{2}} e^{i\pi\hat{S}_{1x}} e^{i\pi\hat{S}_{2y}} e^{i\frac{\pi}{2}\hat{S}_{1x}}
= e^{i\frac{\pi}{4}} e^{-i\frac{\pi}{2}\hat{S}_{2y}} e^{-i\hat{H}_{3}\frac{\tau}{2}} e^{i\pi\hat{S}_{1x}} e^{i\pi\hat{S}_{2y}} e^{-i\hat{H}_{3}\frac{\tau}{2}} e^{-i\pi\hat{S}_{1x}} e^{-i\pi\hat{S}_{2y}} e^{i\frac{\pi}{2}\hat{S}_{1x}}
= e^{i\frac{\pi}{4}} e^{-i\frac{\pi}{2}\hat{S}_{2y}} e^{-i\hat{H}_{3}\frac{\tau}{2}} e^{i\pi\hat{S}_{1x}} e^{i\pi\hat{S}_{2y}} e^{-i\hat{H}_{3}\frac{\tau}{2}} e^{-i\frac{\pi}{2}\hat{S}_{1x}} e^{-i\pi\hat{S}_{2y}}$$
(57)

yielding the following five pulse sequence:

$$180_{2u}^{\circ}, 90_{1x}^{\circ}, \tau_1, 180_{-2u}^{\circ}, 180_{-1x}^{\circ}, \tau_2, 90_{2u}^{\circ}$$
 (58)

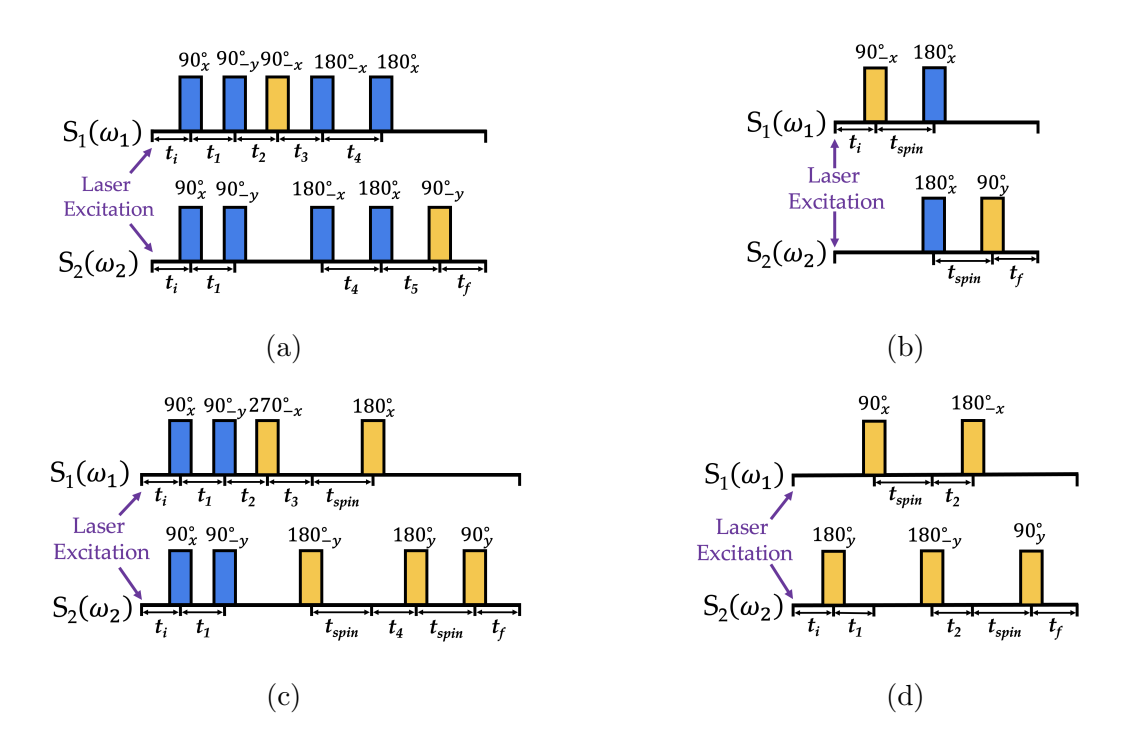


Figure 2: Depiction of pulse EPR experiments for implementation of the CNOT gate. (a), (b) show pulse sequences for \hat{H}_2 in Eq. 11, and (b), (d) show pulse sequences for \hat{H}_3 in Eq. 12. (a) the pulse sequence in Eq. 32 with added correction in Eq. 36, (b) is the sequence in Eq. 59, (c) is the sequence in Eq. 32 with correction in Eq. 38 and (d) is the sequence in Eq. 58. (a),(c) show universal quantum logic gates and (b), (d) show quantum logic gates when the initial state is $|S\rangle$. Each line corresponds to an electron with a Zeeman coupling strength of ω_i , frequency at which selective pulses are centred around. t_i is initial time needed after laser excitation for the formation of the radical pair, t_f is the final time needed between the end of the CNOT gate and read out, t_{spin} are spin evolution times and the remaining times are intervals between pulses. The blue pulses are non-selective rotations for S_1 and S_2 electrons, and yellow pulses are selective rotations.

V. ANALYTICAL DERIVATIONS OF FIDELITY VALUES

Considering ideal pulses, we have derived in this section a number of functions that detail how the fidelity value would vary with time propagation and T_2 relaxation time. They provide a useful way to quantify the dynamics involved in application of a CNOT gate and what results when the pulses in an experiment are non-ideal. Two cases were investigated: pulse sequences in Eq. 56 with \hat{H}_2 for spin evolution, and 58 with \hat{H}_3 for spin evolution. Finally, an upper bound will be given to the fidelity value for these systems that predicts the theoretical maximum possible for a gate given a T_2 relaxation time. Derivations are shown in Appendix C (without T_2) and Appendix D (with T_2 and the upper bound).

A. Fidelity for CNOT Gate Pulse Sequences

At first, fidelity \mathcal{F}_{3P} for the three pulse sequence with arbitrary spin evolution times τ_1 , τ_2 is:

$$\mathcal{F}_{3P} = \frac{1}{4} \left(\cos^2 \left(\frac{\Delta \omega}{2} \left(\tau_1 - \tau_2 \right) \right) + \cos^2 \left(\frac{\Omega}{2} \left(\tau_1 - \tau_2 \right) \right) \right.$$
$$\left. - 2 \sin \left(\frac{\mathcal{D}_1}{2} \left(\tau_1 + \tau_2 \right) \right) \cos \left(\frac{\Delta \omega}{2} \left(\tau_1 - \tau_2 \right) \right) \cos \left(\frac{\Omega}{2} \left(\tau_1 - \tau_2 \right) \right) \right)$$
(59)

When $\tau_1 = \tau_2$, \mathcal{F}_{3P} simplifies to:

$$\mathcal{F}_{3P} = \frac{1}{2} \left(1 - \sin \left(\frac{\mathcal{D}_1}{2} \tau \right) \right) \tag{60}$$

As predicted by the derivations, $\mathcal{F}_{3P} = 1$ when $\tau = \pi/\mathcal{D}_1$. Additionally, this equation would predict the dynamics for the case when \hat{H}_1 would be used for time propagation.

Fidelity \mathcal{F}_{5P} for the five pulse sequence:

$$\mathcal{F}_{5P} = \frac{1}{8} \left(1 + \sin^2 \left(\frac{\Theta}{2} (\tau_1 - \tau_2) \right) \cos(4\xi) + 2\cos^2 \left(\frac{\Omega}{2} (\tau_1 - \tau_2) \right) + \cos^2 \left(\frac{\Theta}{2} (\tau_1 - \tau_2) \right) \right)$$

$$+ 4\cos \left(\frac{\Omega}{2} (\tau_1 - \tau_2) \right) \left(\cos \left(\frac{\mathcal{D}_1}{2} (\tau_1 + \tau_2) \right) \cos(2\xi) \sin \left(\frac{\Theta}{2} (\tau_1 - \tau_2) \right) \right)$$

$$- \sin \left(\frac{\mathcal{D}_1}{2} (\tau_1 + \tau_2) \right) \cos \left(\frac{\Theta}{2} (\tau_1 - \tau_2) \right) \right)$$

$$(61)$$

 \mathcal{F}_{5P} has a very similar form to \mathcal{F}_{3P} and also reduces to Eq. 60 when $\tau_1 = \tau_2$. As predicted by the derivation, when $\tau_1 = \tau_2 = \pi/(2\mathcal{D}_1)$, $\mathcal{F}_{5P} = 1$.

The fidelity equations with T_2 are almost identical to Eqs. 59, 61, the only difference being that some terms are multiplied by $e^{-\tau/T_2}$. They can be seen in Appendix D.

To recapitulate, these equations predict the fidelity value for a system with any number of nuclear spins whose influence on the dynamics will be cancelled out due to the applied pulse sequence.

B. Upper Bound to Fidelity

It is shown in Appendix D that both \mathcal{F}_{3P} and \mathcal{F}_{5P} will be bounded by:

$$\frac{1}{2} + \frac{1}{2}e^{-\frac{\tau}{T_2}} \ge \mathcal{F}\left(\mathcal{D}_1, \mathcal{D}_2, \tau_1, \tau_2, \Delta\omega, \Omega, T_2\right) \tag{62}$$

Here τ is the total gate time, i.e. $\tau = \tau_1 + \tau_2$.

This provides a clear understanding of what would be the best values for certain experiments. For instance, maximum \mathcal{F} values for varying T_2 for the model system are shown in Table II. For the model system, $\pi/|\mathcal{D}_1| = 142.9 \ ns$. The table illustrates that for high T_2 , \mathcal{F} values around 0.9 or even higher can be achieved.

	$T_2 = 1 \ \mu s$	$T_2 = 2 \ \mu s$	$T_2 = 4 \ \mu s$	$T_2 = 8 \ \mu s$
$\tau = \frac{\pi}{2 \mathcal{D}_1 }$	0.9310	0.9649	0.9823	0.9911
$ au = rac{\pi}{ \mathcal{D}_1 }$	0.8668	0.9310	0.9649	0.9823
$\tau = \frac{2\pi}{ \mathcal{D}_1 }$	0.7514	0.8668	0.9310	0.9649
$ au = rac{4\pi}{ \mathcal{D}_1 }$	0.5646	0.7514	0.8668	0.9310

Table II: Maximum \mathcal{F} values (in the middle) for various T_2 and τ for a model SCRP system, for which $\pi/|\mathcal{D}_1| = 142.9 \ ns$.

Two parameters ultimately determine the fidelity of the CNOT gate application, both larger values of \mathcal{D}_1 and longer T_2 relaxation times produce higher fidelity values. It follows that future engineering of these systems should be aimed at maximizing both of these parameters because theoretically such systems could access fidelity values > 0.9.

VI. SIMULATIONS OF THE EXPERIMENTS

A. Model System

We will introduce a model SCRP system **TTF-ANI-PI**, which consists of a tetrathia-fulvalene (**TTF**) electron donor, a 4-amino-1,8-naphthalimide (**ANI**) chromophoric acceptor, and a pyromellitimide (**PI**) secondary acceptor that will be the basis for a computational analysis and has the necessary parameters for calculations already reported in the literature.^{2,38–41} The structure of **TTF-ANI-PI** molecule can be seen in Fig. 3.

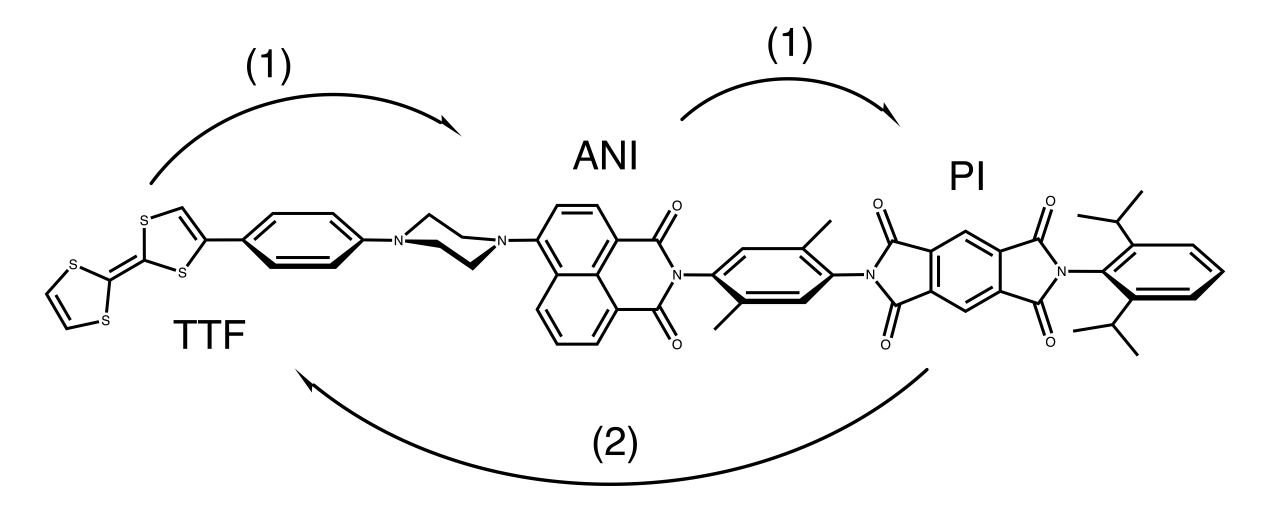


Figure 3: Molecular structure of **TTF-ANI-PI** with outlined forward electron transfers (1), after initial photoexcitation, and backward electron transfer (2), during charge recombination. Adapted from Ref. 2.

Following laser excitation of **TTF-ANI-PI**, a rapid two-step electron transfer produces a SCRP in an initial $|S\rangle$ state. The radical cation is localised on the **TTF** while the radical anion is on the **PI**. The lifetime of the SCRP is sufficiently long (charge recombination lifetime $\tau_{CR} = 35.6 \ \mu s^2$), as well as spin-spin relaxation lifetime ($T_2 = 1.8 \ \mu s^2$ but for simplicity $T_2 = 2 \ \mu s$ will be used throughout the work), to be able to perform quantum gate operations. The g-tensor ($[g_{xx} \ g_{yy} \ g_{zz}]$) for TTF^{•+} is [2.0159 2.0076 2.0031]² and for PI^{•-} is [2.0069 2.0069 2.0021].² The g value in calculations will be the x-component of the full tensor since the molecule is in a single orientation that aligns the dipolar axis, magnetic field vector and the x-axis of the g-tensor. This molecular design was chosen in order to exploit the g-value difference to perform qubit selective rotations. Moreover, the literature

spin - spin coupling values are $\mathcal{D}_1 = -3.50$ MHz and J is taken to be much smaller than \mathcal{D}_1 .⁴¹ The dipolar interaction axis lies approximately parallel to the applied magnetic field direction, i.e. $\theta = 0$. Lastly, the radical around PI moiety will be defined as the target qubit, whereas TTF will be the control qubit. This choice is arbitrary and can be tailored to each experiment.

There are a number of magnetically active nuclei in this system that will give rise to hyperfine couplings to the electron spins. Thus, it is important to quantify their effect on the dynamics. Isotropic hyperfine couplings for TTF^{•+} and PI^{•-} radicals (structure and atom labels are shown in Fig. 4) calculated by Density Functional Theory (DFT) are shown in Table III. The B3LYP functional,^{42,43} def2-TZVP basis set^{44,45} and D3BJ dispersion correction^{46–48} were used for geometry optimization, while the BP86 functional,⁴⁹ EPR-III basis set for PI^{•-50} and cc-PV5Z basis set^{51,52} for TTF^{•+} were used to calculate the hyperfine parameters. These calculations were done with ORCA.^{53,54} These values are not expected to be accurate compared to the experimentally determined values (especially for TTF^{•+} that contains sulphur for which hyperfine optimized EPR-III cannot be used and we had to use hyperfine-unoptimized cc-PV5Z)⁵⁵, and only provide qualitative comparison to the spin-spin coupling. We will compare spin-spin coupling with the effective hyperfine field for radical i:⁵⁶

$$B_{hyp,i} = \sqrt{\sum_{k=1}^{N_i} a_{ik}^2 I_{ik} (I_{ik} + 1)}$$
(63)

Here a_{ik} are isotropic hyperfine constants for nuclei k coupled to electron i.

For TTF^{•+}, $B_{hyp,1} = 6.0539$ MHz, and for PI^{•-}, $B_{hyp,2} = 5.4799$ MHz. Since the magnitude of the effective hyperfine fields are in the order of magnitude of \mathcal{D}_1 , it is vital to understand the influence of hyperfine interactions on the spin dynamics of applying quantum logic gates.

Molecule Nuclei a_{iso} / MHz				
	H1	-3.32		
$\mathrm{TTF}^{\bullet+}$	H2	-3.19		
	НЗ	-5.26		
	H1	1.46		
PI^{ullet-}	H2	1.46		
	N1	-2.59		
	N2	-2.59		

Table III: Isotropic hyperfine interaction parameters in MHz for TTF^{•+} and PI^{•−} radicals, which structures and atom labels are shown in Fig. 4.

$$\begin{bmatrix} N1 & H1 & N2 \\ H-N & H2 & N-H \\ & & & & \\ & & & & \\ & & & & \\ & & & & \\ & & & & \\ & & & & \\ & & & & \\ & & & & \\ & & & & \\ & & & & \\ & & &$$

Figure 4: Structures of (a) $PI^{\bullet-}$ and (b) $TTF^{\bullet+}$ that were used to calculate the isotropic hyperfine coupling constants given in Table III. Atom labels highlight magnetically important nuclei that have non-zero spin.

B. Simulations

Using the parameters obtained for **TTF-ANI-PI**, the fidelity following application of a CNOT gate under varying magnetic field conditions was simulated. Typically, EPR experiments are performed at X-band (9.5 GHz) or higher. We will first simulate the three pulse sequence at 9.5 GHz, which is high enough to invoke the weak coupling approximation and for the use of Eq. 36 for spin evolution. The simulation of Eq. 59 without T_2 relaxation at 9.5 GHz is shown in Fig. 5a. The value of τ_1 is held constant at $\tau_1 = \pi/(2\mathcal{D}_1) = 71.43 \ ns$

(optimal value according to theory) and τ_2 is varied from 0 to $\pi/|\mathcal{D}_1|$. There is a very fast oscillation in the fidelity, for which the principal driving factor is the sum of the electron Zeeman splitting, Ω , introducing a period of T=0.0523~ns. The period of all of the important motions at this microwave frequency are summarized in Table IV. In a real experiment, pulses will not be ideal and spectral inhomogeneities will make it impossible to replicate $\tau_1 = \tau_2 = \pi/(2\mathcal{D}_1)$, where the maximum is theorized to occur. One solution is working at a lower magnetic field strength. For instance, if the field is lowered by 20 times from the X-band value, then the resonance frequency is about 0.475 GHz and the period for Ω would be T=1.05~ns, which is a more realistic timing parameter for digital electronics. The graph of \mathcal{F}_{5P} for this magnetic field strength, with \hat{H}_3 for spin evolution is shown in Fig. 5b.

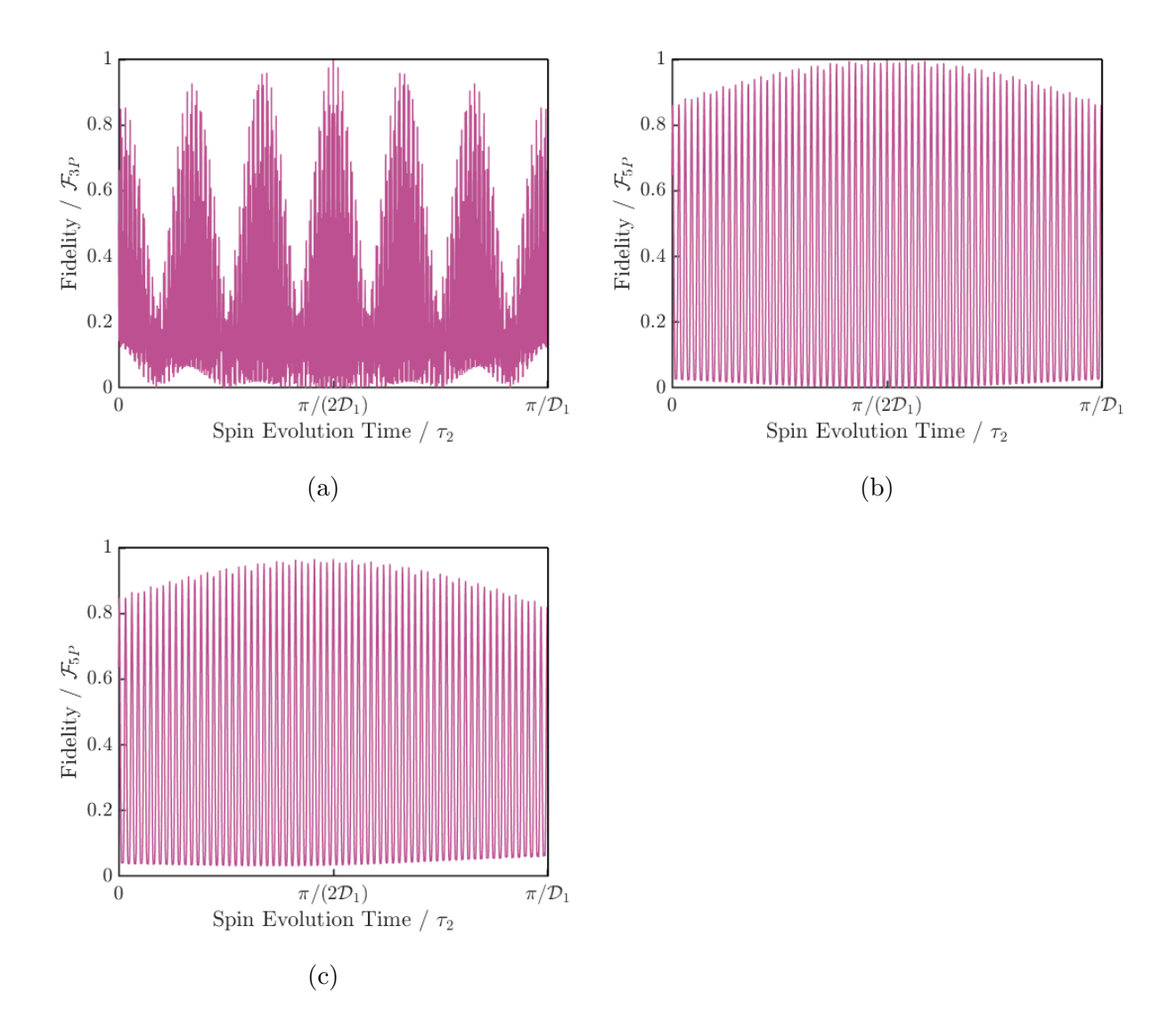


Figure 5: Graphs of fidelity versus spin evolution time for model system introduced in Sec. VI A. (a) uses Eq. 59 for fidelity and \hat{H}_2 in Eq. 11 for spin evolution. (b), (c) uses Eq. 59 for fidelity and \hat{H}_3 in Eq. 12 for spin evolution. Case (c) has T_2 relaxation included. The resonance frequency is 9.5 GHz for (a) and 0.475 GHz for (b) and (c). In all cases, $\tau_1 = \pi/(2|\mathcal{D}_1|) = 71.43 \ ns$ and τ_2 is varied from 0 to $\pi/|\mathcal{D}_1| = 142.9 \ ns$.

Also, it can be seen that the fidelity values are relatively high for this case before $\tau_2 = \pi/\mathcal{D}_2$ and since T_2 will decrease \mathcal{F}_{5P} values with total time τ , we note that it is possible to achieve a maximum earlier when decoherence effects are taken into account. Fig. 5c shows the same graph as Fig. 5b but with T_2 relaxation included and the maximum for this graph occurs at $\tau_2 = 65.14$ ns and it is $\mathcal{F}_{3P} = 0.9658$, which brings down the total time to $\tau = 136.57$ ns. This result exemplifies the fact that a better understanding of the spin

dynamics results in ways to reduce the total gate times.

Term	Frequency	Period
$ \Omega $	19.11 GHz	$0.0523 \ ns$
$\left \frac{\Omega}{2}\right $	9.56 GHz	0.105~ns
$ \Delta\omega $	42.7 MHz	23.4~ns
$\left \frac{\Delta \omega}{2} \right $	21.4 MHz	46.7~ns
$\left \frac{\mathcal{D}_1}{2}\right $	1.75 MHz	571.4 ns

Table IV: Frequencies and periods of oscillatory motions in \mathcal{F}_{3P} functions in Eqs. 59 at a 9.5 GHz resonance frequency.

Even though, the majority of issues of implementing quantum logic gates for these systems are alleviated at lower magnetic field values, engineering pulses for these magnetic field values propose another challenge. The spectral separation of the EPR lines of the two radicals will be reduced at lower magnetic fields, so that their linewidths will be larger than their separation, prohibiting the selective rotations that are necessary for the quantum logic gate operations. Hence, designing new SCRPs in which hyperfine interactions are minimized or eliminated and that can also be ordered in crystalline environments, may provide the required linewidth reductions. In addition, alternative experimental protocols, such as those done with the Gradient Ascent Pulse Engineering (GRAPE) approach, ^{57–59} may prove beneficial. Nonetheless, our results indicate that a lower magnetic field may be a prerequisite for controlling the spin states in these systems for QIS applications or that there is a need for methods to alleviate the fast oscillations from the dynamics.

VII. CONCLUSIONS

In this article we introduced a variety of advances in pulse protocols for executing two qubit quantum logic gates on SCRP systems and provided the theoretical framework for understanding the dynamics of applying them to experiments. Specifically, we introduced pulse sequences for CNOT, SWAP, CZ and CP gates that have the correct signs for the spin propagation term. In addition, we have introduced corrections for the Hamiltonians in Eqs.

11, 12 in terms of extra pulse sequences, illustrating how these corrections cancel out static hyperfine interactions from the dynamics, and how with a simplification for a singlet initial state we can execute the CNOT gate in either 3 or 5 pulses. This is an improvement from the previous state of the art and will enable new experiments to be executed that will utilize these quantum logic gates. Lastly, a theoretical treatment was given for fidelity values for varying spin evolution times and a set of analytical equations were derived for both three and five pulse experiments. These equations highlight the upper bound for fidelity values that is imposed by T_2 relaxation and what are the important factors in the dynamics that control the fidelity value. As a main conclusion, we have shown that high fidelity values are possible for these systems, yet the resonance frequency has to be lower than the 9.5 GHz value typical of X-band to ensure that the fast oscillations have a long enough period for control.

There are many possible future directions of research that this study did not address, e.g. simulations with realistic pulses, executing selective rotations at lower magnetic fields, theoretical treatments of echo detection, proposals of new ways to do quantum state tomography for this system, using GRAPE for executing quantum logic gates, understanding how radical recombination affects the performance of the gate action, dynamic decoupling or other schemes to make the gate execution easier and so on. Also, experimentally testing these pulse sequences for different systems, magnetic field values and different pulse shapes will shed light on future research directions. Lastly, we are currently planning to use these new pulse sequences in experimental studies on several newly designed SCRP systems suitable for QIS applications.

VIII. ACKNOWLEDGEMENTS

GJP is grateful to the European Research Council (under the European Unions Horizon 2020 research and innovation programme, Grant Agreement No. 810002, Synergy Grant: QuantumBirds). This research was supported by the US National Science Foundation under award no. CHE-2154627 (M.R.W.).

Appendix A: Commutation of Hamiltonians with Hyperfine Interaction Terms

First, we will derive $\left[\hat{H}_{hyp,2}, \hat{H}'_{hyp,2}\right]$, where

$$\hat{H}_{hyp,2} = \hat{H}_2 + \hat{H}_{hyp} \tag{A1}$$

$$\hat{H}'_{hyp,2} = \hat{H}'_2 - \hat{H}_{hyp} \tag{A2}$$

Hence, by using properties of commutators we find that:

By plugging in definitions of \hat{H}_2 , \hat{H}_2' and \hat{H}_{hyp} :

The final result is zero because nuclear spin operators commute freely with electron spin operators, hence, the final line is identical to the $\left[\hat{S}_{1z}+\hat{S}_{2z},\mathcal{D}_1\hat{S}_{1z}\hat{S}_{2z}\right]$ result, i.e. 0.

Evaluating $\left[\hat{H}_{hyp,3},\hat{H}'_{hyp,3}\right]$ has equivalent initial steps and we find that:

$$\begin{split} \left[\hat{H}_{hyp,3}, \hat{H}'_{hyp,3}\right] &= \left[\hat{H}_{hyp}, \omega_{1} \hat{S}_{1z} + \omega_{2} \hat{S}_{2z} + \mathcal{D}_{1} \hat{S}_{1z} \hat{S}_{2z} + \mathcal{D}_{2} \left(\hat{S}_{1x} \hat{S}_{2x} + \hat{S}_{1y} \hat{S}_{2y}\right)\right] \\ &+ \left[\hat{H}_{hyp}, -\omega_{1} \hat{S}_{1z} - \omega_{2} \hat{S}_{2z} + \mathcal{D}_{1} \hat{S}_{1z} \hat{S}_{2z} - \mathcal{D}_{2} \left(\hat{S}_{1x} \hat{S}_{2x} + \hat{S}_{1y} \hat{S}_{2y}\right)\right] \\ &= \left[\hat{H}_{hyp}, \omega_{1} \hat{S}_{1z}\right] + \left[\hat{H}_{hyp}, \omega_{2} \hat{S}_{2z}\right] + \left[\hat{H}_{hyp}, \mathcal{D}_{1} \hat{S}_{1z} \hat{S}_{2z}\right] + \left[\hat{H}_{hyp}, \mathcal{D}_{2} \left(\hat{S}_{1x} \hat{S}_{2x} + \hat{S}_{1y} \hat{S}_{2y}\right)\right] \\ &- \left[\hat{H}_{hyp}, \omega_{1} \hat{S}_{1z}\right] - \left[\hat{H}_{hyp}, \omega_{2} \hat{S}_{2z}\right] + \left[\hat{H}_{hyp}, \mathcal{D}_{1} \hat{S}_{1z} \hat{S}_{2z}\right] - \left[\hat{H}_{hyp}, \mathcal{D}_{2} \left(\hat{S}_{1x} \hat{S}_{2x} + \hat{S}_{1y} \hat{S}_{2y}\right)\right] \\ &= 2\left[\hat{H}_{hyp}, \mathcal{D}_{1} \hat{S}_{1z} \hat{S}_{2z}\right] = 0 \end{split}$$

(A5)

Appendix B: Derivations of Pulse Sequences

1. SWAP Gate

The expression for the SWAP gate found by the expansion in Eq. 16:

$$\hat{U}_{SWAP} = E_{+}^{1,2} + 4\hat{S}_{1x}\hat{S}_{2x}E_{-}^{1,2} \tag{B1}$$

This can further be decomposed to:

$$\hat{U}_{SWAP} = E_{+}^{1,2} + 4\hat{S}_{1x}\hat{S}_{2x}E_{-}^{1,2}
= \left(iE_{-}^{1,2} + E_{+}^{1,2}\right) \left(-4i\hat{S}_{1x}\hat{S}_{2x}E_{-}^{1,2} + E_{+}^{1,2}\right)
= e^{i\frac{\pi}{2}E_{-}^{1,2}}e^{-i2\pi\hat{S}_{1x}\hat{S}_{2x}E_{-}^{1,2}}$$
(B2)

We notice that,

$$\hat{S}_{1x}\hat{S}_{2x}E_{-}^{1,2} = \hat{S}_{1x}\hat{S}_{2x}\left(\frac{1}{2}\mathbb{I} - 2\hat{S}_{1z}\hat{S}_{2z}\right) = \frac{1}{2}\hat{S}_{1x}\hat{S}_{2x} - 2\hat{S}_{1x}\hat{S}_{2x}\hat{S}_{1z}\hat{S}_{2z} = \frac{1}{2}\hat{S}_{1x}\hat{S}_{2x} + \frac{1}{2}\hat{S}_{1y}\hat{S}_{2y}$$
(B3)

Hence, the unitary for the SWAP gate is:

$$\hat{U}_{SWAP} = e^{i\frac{\pi}{4}} e^{-i\pi \hat{S}_{1z} \hat{S}_{2z}} e^{-i\pi \hat{S}_{1x} \hat{S}_{2x}} e^{-i\pi \hat{S}_{1y} \hat{S}_{2y}}$$
(B4)

We do not have the right sign for the $\hat{S}_{1z}\hat{S}_{2z}$ operator, hence, we can take a Hermitian conjugate to get the right sign:

$$\hat{U}_{SWAP}^{\dagger} = \hat{U}_{SWAP} = e^{-i\frac{\pi}{4}} e^{i\pi \hat{S}_{1y} \hat{S}_{2y}} e^{i\pi \hat{S}_{1x} \hat{S}_{2x}} e^{i\pi \hat{S}_{1z} \hat{S}_{2z}}$$
(B5)

We can decompose the x and y terms as:

$$e^{i\pi\hat{S}_{1x}\hat{S}_{2x}} = e^{i\frac{\pi}{2}(\hat{S}_{1y} + \hat{S}_{2y})} e^{i\pi\hat{S}_{1z}\hat{S}_{2z}} e^{-i\frac{\pi}{2}(\hat{S}_{1y} + \hat{S}_{2y})}$$
(B6)

$$e^{i\pi\hat{S}_{1y}\hat{S}_{2y}} = e^{i\frac{\pi}{2}(\hat{S}_{1x} + \hat{S}_{2x})} e^{i\pi\hat{S}_{1z}\hat{S}_{2z}} e^{-i\frac{\pi}{2}(\hat{S}_{1x} + \hat{S}_{2x})}$$
(B7)

Hence, the final unitary:

$$\hat{U}_{SWAP} = e^{-i\frac{\pi}{4}} e^{i\pi \hat{S}_{1z} \hat{S}_{2z}} e^{i\frac{\pi}{2} (\hat{S}_{1y} + \hat{S}_{2y})} e^{i\pi \hat{S}_{1z} \hat{S}_{2z}} e^{-i\frac{\pi}{2} (\hat{S}_{1y} + \hat{S}_{2y})} e^{i\frac{\pi}{2} (\hat{S}_{1x} + \hat{S}_{2x})} e^{i\pi \hat{S}_{1z} \hat{S}_{2z}} e^{-i\frac{\pi}{2} (\hat{S}_{1x} + \hat{S}_{2x})}$$
(B8)

Pulse Sequence:

$$90_{1x+2x}^{\circ}, \frac{\pi}{|\mathcal{D}_{1}|}, 90_{-(1x+2x)}^{\circ}, 90_{1y+2y}^{\circ}, \frac{\pi}{|\mathcal{D}_{1}|}, 90_{-(1y+2y)}^{\circ}, \frac{\pi}{|\mathcal{D}_{1}|}$$
 (B9)

2. CZ gate

The expression for the CZ gate found by the expansion in Eq. 16:

$$\hat{U}_{CZ} = 2\hat{S}_{2z}E_{-}^{1} + E_{+}^{1} \tag{B10}$$

Note that:

$$2\hat{S}_{2z} = e^{i\pi(\frac{1}{2}\mathbb{I} - \hat{S}_{2z})} = e^{-i\pi E_{-}^{2}}$$
(B11)

Hence,

$$\hat{U}_{CZ} = e^{-i\pi E_{-}^{2}} E_{-}^{1} + E_{+}^{1} = e^{-i\pi E_{-}^{2}} E_{-}^{1} = e^{-i\pi E_{-}^{1}} E_{-}^{2}$$
(B12)

 $E_{-}^{1}E_{-}^{2}$ is equal to:

$$E_{-}^{1}E_{-}^{2} = \left(\frac{1}{2}\mathbb{I} - \hat{S}_{1z}\right) \left(\frac{1}{2}\mathbb{I} - \hat{S}_{2z}\right)$$

$$= \frac{1}{4}\mathbb{I} - \frac{1}{2}\hat{S}_{1z} - \frac{1}{2}\hat{S}_{2z} + \hat{S}_{1z}\hat{S}_{2z}$$
(B13)

Plugging it into the exponent:

$$\hat{U}_{CZ} = e^{-i\frac{\pi}{4}} e^{i\frac{\pi}{2}\hat{S}_{1z}} e^{i\frac{\pi}{2}\hat{S}_{2z}} e^{-i\pi\hat{S}_{1z}\hat{S}_{2z}}$$
(B14)

The minus sign on the $\hat{S}_{1z}\hat{S}_{2z}$ is a problem, hence we will take the hermitian conjugate of this operator (which will leave it unchanged):

$$\hat{U}_{CZ}^{\dagger} = \hat{U}_{CZ} = e^{i\frac{\pi}{4}} e^{i\pi\hat{S}_{1z}\hat{S}_{2z}} e^{-i\frac{\pi}{2}\hat{S}_{2z}} e^{-i\frac{\pi}{2}\hat{S}_{1z}}$$
(B15)

There are different ways to expand the \hat{S}_{1z} and \hat{S}_{2z} , yet one of the ways:

$$e^{-i\frac{\pi}{2}\hat{S}_{1z}} = e^{-i\frac{\pi}{2}\hat{S}_{1x}}e^{-i\frac{\pi}{2}\hat{S}_{1y}}e^{i\frac{\pi}{2}\hat{S}_{1x}}$$
(B16)

$$e^{-i\frac{\pi}{2}\hat{S}_{2z}} = e^{i\frac{\pi}{2}\hat{S}_{2y}}e^{-i\frac{\pi}{2}\hat{S}_{2x}}e^{-i\frac{\pi}{2}\hat{S}_{2y}}$$
(B17)

The final unitary for the CZ gate:

$$\hat{U}_{CZ} = e^{i\frac{\pi}{4}} e^{i\pi\hat{S}_{1z}\hat{S}_{2z}} e^{-i\frac{\pi}{2}\hat{S}_{2z}} e^{-i\frac{\pi}{2}\hat{S}_{1z}}
= e^{i\frac{\pi}{4}} e^{i\pi\hat{S}_{1z}\hat{S}_{2z}} e^{i\frac{\pi}{2}\hat{S}_{2y}} e^{-i\frac{\pi}{2}\hat{S}_{2x}} e^{-i\frac{\pi}{2}\hat{S}_{2y}} e^{-i\frac{\pi}{2}\hat{S}_{1x}} e^{-i\frac{\pi}{2}\hat{S}_{1y}} e^{i\frac{\pi}{2}\hat{S}_{1x}}
= e^{i\frac{\pi}{4}} e^{i\pi\hat{S}_{1z}\hat{S}_{2z}} e^{i\frac{\pi}{2}\hat{S}_{2y}} e^{-i\frac{\pi}{2}(\hat{S}_{1x}+\hat{S}_{2x})} e^{-i\frac{\pi}{2}(\hat{S}_{1y}+\hat{S}_{2y})} e^{i\frac{\pi}{2}\hat{S}_{1x}}$$
(B18)

This reproduces the correct gate action, and the pulse sequence is:

$$90^{\circ}_{-1x}, \ 90^{\circ}_{1y+2y}, \ 90^{\circ}_{1x+2x}, \ 90^{\circ}_{-2y}, \ \frac{\pi}{|\mathcal{D}_1|}$$
 (B19)

3. CP Gate

A general CP gate for controlling phase of the $|\beta\beta\rangle$ state:

$$\hat{U}_{CP}(\phi) = \begin{pmatrix} 1 & 0 & 0 & 0 \\ 0 & 1 & 0 & 0 \\ 0 & 0 & 1 & 0 \\ 0 & 0 & 0 & e^{i\phi} \end{pmatrix}$$
(B20)

A decomposition of the propagation matrix into rotation matrices:⁶⁰

$$\hat{U}_{CP}(\phi) = e^{i\frac{\phi}{4}\mathbb{I}} e^{-i\frac{\phi}{2}\hat{S}_{1z}} e^{-i\frac{\phi}{2}\hat{S}_{2z}} e^{i\phi\hat{S}_{1z}\hat{S}_{2z}} = e^{i\frac{\phi}{4}} e^{i\phi\hat{S}_{1z}\hat{S}_{2z}} e^{-i\frac{\phi}{2}\hat{S}_{1z}} e^{-i\frac{\phi}{2}\hat{S}_{2z}}$$
(B21)

The \hat{S}_{1z} and \hat{S}_{2z} exponents can be written as:

$$e^{-i\frac{\phi}{2}\hat{S}_{1z}} = e^{-i\frac{\pi}{2}\hat{S}_{1y}}e^{i\frac{\phi}{2}\hat{S}_{1x}}e^{i\frac{\pi}{2}\hat{S}_{1y}}$$
(B22)

$$e^{-i\frac{\phi}{2}\hat{S}_{2z}} = e^{i\frac{\pi}{2}\hat{S}_{2x}}e^{i\frac{\phi}{2}\hat{S}_{2y}}e^{-i\frac{\pi}{2}\hat{S}_{2x}}$$
(B23)

The final CP gate:

$$\hat{U}_{CP}(\phi) = e^{i\phi \hat{S}_{1z} \hat{S}_{2z}} e^{-i\frac{\phi}{2} \hat{S}_{1z}} e^{-i\frac{\phi}{2} \hat{S}_{2z}}
= e^{i\phi \hat{S}_{1z} \hat{S}_{2z}} e^{-i\frac{\pi}{2} \hat{S}_{1y}} e^{i\frac{\phi}{2} \hat{S}_{1x}} e^{i\frac{\pi}{2} \hat{S}_{1y}} e^{i\frac{\pi}{2} \hat{S}_{2x}} e^{i\frac{\phi}{2} \hat{S}_{2y}} e^{-i\frac{\pi}{2} \hat{S}_{2x}}$$
(B24)

Hence, the general pulse sequence is:

$$90_{2x}^{\circ}, \left(\frac{\phi}{2}\right)_{-2y}^{\circ}, 90_{-2x}^{\circ}, 90_{-1y}^{\circ}, \left(\frac{\phi}{2}\right)_{-1x}^{\circ}, 90_{1y}^{\circ}, \frac{\phi}{|\mathcal{D}_{1}|}$$
 (B25)

Appendix C: Derivations of Fidelity Equations

Two cases will be derived in this section—the fidelity equation for the three pulse sequence in Eq. 56 with \hat{H}_2 in Eq. 11 for spin evolution and equation for the five pulse sequence in Eq. 58 with \hat{H}_3 for spin evolution. In each case, the fidelity definition in Eq. 22 will be used. Both pulse sequences have two spin evolution times, these will be set as arbitrary propagation times τ_1 and τ_2 ,

1. Three Pulse Sequence

The \hat{H}_2 in matrix form (in $|\alpha\alpha\rangle$, $|\alpha\beta\rangle$, $|\beta\alpha\rangle$, $|\beta\beta\rangle$ basis):

$$\hat{H}_{2} = \begin{pmatrix} \langle \alpha \alpha | \hat{H}_{2} | \alpha \alpha \rangle & 0 & 0 & 0 \\ 0 & \langle \alpha \beta | \hat{H}_{2} | \alpha \beta \rangle & 0 & 0 \\ 0 & 0 & \langle \beta \alpha | \hat{H}_{2} | \beta \alpha \rangle & 0 \\ 0 & 0 & 0 & \langle \beta \beta | \hat{H}_{2} | \beta \beta \rangle \end{pmatrix}$$
(C1)

Where,

$$\langle \alpha \alpha | \hat{H}_{2} | \alpha \alpha \rangle = H_{1} = \frac{1}{2} (\omega_{1} + \omega_{2}) + \frac{\mathcal{D}_{1}}{4} = \frac{\Omega}{2} + \frac{\mathcal{D}_{1}}{4}$$

$$\langle \alpha \beta | \hat{H}_{2} | \alpha \beta \rangle = H_{2} = \frac{1}{2} (\omega_{1} - \omega_{2}) - \frac{\mathcal{D}_{1}}{4} = -\frac{\Delta \omega}{2} - \frac{\mathcal{D}_{1}}{4}$$

$$\langle \beta \alpha | \hat{H}_{2} | \beta \alpha \rangle = H_{3} = \frac{1}{2} (\omega_{2} - \omega_{1}) - \frac{\mathcal{D}_{1}}{4} = \frac{\Delta \omega}{2} - \frac{\mathcal{D}_{1}}{4}$$

$$\langle \beta \beta | \hat{H}_{2} | \beta \beta \rangle = H_{4} = -\frac{1}{2} (\omega_{1} + \omega_{2}) + \frac{\mathcal{D}_{1}}{4} = -\frac{\Omega}{2} + \frac{\mathcal{D}_{1}}{4}$$
(C2)

The time-propagation operator in matrix form:

$$e^{-i\hat{H}_{2}\tau} = \begin{pmatrix} e^{-iH_{1}\tau} & 0 & 0 & 0 \\ 0 & e^{-iH_{2}\tau} & 0 & 0 \\ 0 & 0 & e^{-iH_{3}\tau} & 0 \\ 0 & 0 & 0 & e^{-iH_{4}\tau} \end{pmatrix} = \begin{pmatrix} e^{-i\frac{\Omega}{2}\tau}e^{-i\frac{\mathcal{D}_{1}}{4}\tau} & 0 & 0 & 0 \\ 0 & e^{i\frac{\Delta\omega}{2}\tau}e^{i\frac{\mathcal{D}_{1}}{4}\tau} & 0 & 0 \\ 0 & 0 & e^{-i\frac{\Delta\omega}{2}\tau}e^{i\frac{\mathcal{D}_{1}}{4}\tau} & 0 \\ 0 & 0 & 0 & e^{i\frac{\Omega}{2}\tau}e^{-i\frac{\mathcal{D}_{1}}{4}\tau} \end{pmatrix}$$

$$(C3)$$

Hence, \mathcal{F}_{3P} for the three pulse sequence:

$$\mathcal{F}_{3P} = \left| \langle S | \hat{U}_{spin}^{\dagger} \hat{U}_{CNOT} | S \rangle \right|^{2}$$

$$= \left| \langle S | \left(e^{i\frac{\pi}{4}} e^{-i\frac{\pi}{2} \hat{S}_{2y}} e^{-\hat{H}_{\frac{\tau_{1}}{2}}^{\tau_{1}}} e^{-i\pi \left(\hat{S}_{1x} + \hat{S}_{2x} \right)} e^{-i\hat{H}_{\frac{\tau_{2}}{2}}^{\tau_{2}}} e^{i\frac{\pi}{2} \hat{S}_{1x}} \right)^{\dagger} \hat{U}_{CNOT} | S \rangle \right|^{2}$$

$$= \frac{1}{16} \left| e^{-i\frac{\Delta\omega}{2}(\tau_{1} - \tau_{2})} e^{i\frac{\mathcal{D}_{1}}{4}(\tau_{1} + \tau_{2})} + e^{i\frac{\Delta\omega}{2}(\tau_{1} - \tau_{2})} e^{i\frac{\mathcal{D}_{1}}{4}(\tau_{1} + \tau_{2})} - i \left(e^{i\frac{\Omega}{2}(\tau_{1} - \tau_{2})} e^{-i\frac{\mathcal{D}_{1}}{4}(\tau_{1} + \tau_{2})} + e^{-i\frac{\Omega}{2}(\tau_{1} - \tau_{2})} e^{-i\frac{\mathcal{D}_{1}}{4}(\tau_{1} + \tau_{2})} \right) \right|^{2}$$

$$= \frac{1}{4} \left(\cos^{2} \left(\frac{\Delta\omega}{2} \left(\tau_{1} - \tau_{2} \right) \right) + \cos^{2} \left(\frac{\Omega}{2} \left(\tau_{1} - \tau_{2} \right) \right) - 2 \sin \left(\frac{\mathcal{D}_{1}}{2} \left(\tau_{1} + \tau_{2} \right) \right) \cos \left(\frac{\Delta\omega}{2} \left(\tau_{1} - \tau_{2} \right) \right) \cos \left(\frac{\Omega}{2} \left(\tau_{1} - \tau_{2} \right) \right) \right)$$

$$= \frac{1}{4} \left(1 + \frac{1}{2} \cos \left(\Delta\omega \left(\tau_{1} - \tau_{2} \right) \right) + \frac{1}{2} \cos \left(\Omega \left(\tau_{1} - \tau_{2} \right) \right) - 2 \sin \left(\frac{\mathcal{D}_{1}}{2} \left(\tau_{1} + \tau_{2} \right) \right) \cos \left(\frac{\Delta\omega}{2} \left(\tau_{1} - \tau_{2} \right) \right) \cos \left(\frac{\Omega}{2} \left(\tau_{1} - \tau_{2} \right) \right) \right)$$

$$-2 \sin \left(\frac{\mathcal{D}_{1}}{2} \left(\tau_{1} + \tau_{2} \right) \right) \cos \left(\frac{\Delta\omega}{2} \left(\tau_{1} - \tau_{2} \right) \right) \cos \left(\frac{\Omega}{2} \left(\tau_{1} - \tau_{2} \right) \right) \right)$$

This equation is maximum, i.e. $\mathcal{F} = 1$, when this set of simultaneous equations is solved:

$$\begin{cases}
\cos\left(\frac{\Delta\omega}{2}(\tau_1 - \tau_2)\right) = \pm 1 \\
\cos\left(\frac{\Omega}{2}(\tau_1 - \tau_2)\right) = \pm 1 \\
\sin\left(\frac{D_1}{2}(\tau_1 + \tau_2)\right) = 1
\end{cases}$$
(C5)

Solutions:

$$\begin{cases}
\tau_1 - \tau_2 = \pm \frac{2\pi k_1}{\Delta \omega} \\
\tau_1 - \tau_2 = \pm \frac{2\pi k_2}{\Omega} \\
\tau_1 + \tau_2 = \frac{\pi}{D_1} + \frac{2\pi k_3}{D_1}
\end{cases}$$
(C6)

 $k_1, k_2, k_3 \in \mathbb{Z}$. If $\tau_1 + \tau_2 = \pi/\mathcal{D}_1$, then solutions for τ_1 and τ_2 :

$$\tau_{1} = \frac{\pi}{2\mathcal{D}_{1}} \pm \frac{\pi k_{1}}{\Delta \omega} = \frac{\pi}{2\mathcal{D}_{1}} \pm \frac{\pi k_{2}}{\Omega}$$

$$\tau_{2} = \frac{\pi}{2\mathcal{D}_{1}} \mp \frac{\pi k_{1}}{\Delta \omega} = \frac{\pi}{2\mathcal{D}_{1}} \mp \frac{\pi k_{2}}{\Omega}$$
(C7)

If $\tau_1 = \tau_2$ and $\tau_1 + \tau_2 = \tau$, then:

$$\mathcal{F} = \frac{1}{2} \left(1 - \sin \left(\frac{\mathcal{D}_1}{2} \tau \right) \right) \tag{C8}$$

This is maximum when $\tau = \pi/\mathcal{D}_1 + 2\pi k/\mathcal{D}_1$ for $k \in \mathbb{Z}$, as expected from derivations.

2. Five Pulse Sequence

 \hat{H}_3 can be decomposed into:

$$\hat{H}_3 = \mathbf{R} \mathbf{A} \mathbf{R}^{-1} \tag{C9}$$

Here,

$$\mathbf{A} = \begin{pmatrix} \lambda_1 & 0 & 0 & 0 \\ 0 & \lambda_2 & 0 & 0 \\ 0 & 0 & \lambda_3 & 0 \\ 0 & 0 & 0 & \lambda_4 \end{pmatrix} \tag{C10}$$

$$\mathbf{R} = \begin{pmatrix} 1 & 0 & 0 & 0 \\ 0 & \frac{1}{\sqrt{2}}(\cos\xi + \sin\xi) & \frac{1}{\sqrt{2}}(\cos\xi - \sin\xi) & 0 \\ 0 & \frac{1}{\sqrt{2}}(\sin\xi - \cos\xi) & \frac{1}{\sqrt{2}}(\cos\xi + \sin\xi) & 0 \\ 0 & 0 & 0 & 1 \end{pmatrix}$$
(C11)

$$\mathbf{R}^{-1} = \begin{pmatrix} 1 & 0 & 0 & 0 \\ 0 & \frac{1}{\sqrt{2}}(\cos\xi + \sin\xi) & \frac{1}{\sqrt{2}}(\sin\xi - \cos\xi) & 0 \\ 0 & \frac{1}{\sqrt{2}}(\cos\xi - \sin\xi) & \frac{1}{\sqrt{2}}(\cos\xi + \sin\xi) & 0 \\ 0 & 0 & 0 & 1 \end{pmatrix}$$
(C12)

The matrix exponential of \hat{H}_3 can be expressed as:

$$e^{-i\hat{H}_{3}\tau} = \mathbf{R}e^{-i\mathbf{A}\tau}\mathbf{R}^{-1} = \begin{pmatrix} H_{11} & 0 & 0 & 0\\ 0 & H_{22} & H_{23} & 0\\ 0 & H_{32} & H_{33} & 0\\ 0 & 0 & 0 & H_{44} \end{pmatrix}$$
(C13)

Where,

$$H_{11} = e^{-i\frac{\Omega}{2}\tau} e^{-i\frac{\mathcal{D}_1}{4}\tau}; \quad H_{44} = e^{i\frac{\Omega}{2}\tau} e^{-i\frac{\mathcal{D}_1}{4}\tau}$$

$$H_{22} = \left(\cos\left(\frac{\Theta}{2}\tau\right) + i\sin(2\xi)\sin\left(\frac{\Theta}{2}\tau\right)\right) e^{i\frac{\mathcal{D}_1}{4}\tau}$$

$$H_{33} = \left(\cos\left(\frac{\Theta}{2}\tau\right) - i\sin(2\xi)\sin\left(\frac{\Theta}{2}\tau\right)\right) e^{i\frac{\mathcal{D}_1}{4}\tau}$$

$$H_{23} = H_{32} = -i\cos(2\xi)\sin\left(\frac{\Theta}{2}\tau\right) e^{i\frac{\mathcal{D}_1}{4}\tau}$$
(C14)

Finally, the \mathcal{F}_{5P} for the five pulse sequence:

$$\mathcal{F}_{5P} = \left| \langle S | \hat{U}_{spin}^{\dagger} \hat{U}_{CNOT} | S \rangle \right|^{2}$$

$$= \frac{1}{4} |z|^{2}$$

$$= \frac{1}{4} \left(\operatorname{Re}(z)^{2} + \operatorname{Im}(z)^{2} \right)$$
(C15)

Where,

$$Re(z) = -\cos\left(\frac{\Omega}{2}(\tau_1 - \tau_2)\right) \sin\left(\frac{\mathcal{D}_1}{4}(\tau_1 + \tau_2)\right) + \cos\left(\frac{\Theta}{2}(\tau_1 - \tau_2)\right) \cos\left(\frac{\mathcal{D}_1}{4}(\tau_1 + \tau_2)\right) + \sin\left(\frac{\Theta}{2}(\tau_1 - \tau_2)\right) \cos(2\xi) \sin\left(\frac{\mathcal{D}_1}{4}(\tau_1 + \tau_2)\right)$$
(C16)

$$\operatorname{Im}(z) = -\cos\left(\frac{\Omega}{2}(\tau_1 - \tau_2)\right)\cos\left(\frac{\mathcal{D}_1}{4}(\tau_1 + \tau_2)\right) + \cos\left(\frac{\Theta}{2}(\tau_1 - \tau_2)\right)\sin\left(\frac{\mathcal{D}_1}{4}(\tau_1 + \tau_2)\right) \\ -\sin\left(\frac{\Theta}{2}(\tau_1 - \tau_2)\right)\cos(2\xi)\cos\left(\frac{\mathcal{D}_1}{4}(\tau_1 + \tau_2)\right)$$
(C17)

The equation after expansion:

$$\mathcal{F}_{5P} = \frac{1}{16} \left(5 - \frac{1}{2} \cos(\Theta(\tau_1 - \tau_2) - 4\xi) - \frac{1}{2} \cos(\Theta(\tau_1 - \tau_2) + 4\xi) \right)$$

$$+ \cos(4\xi) + 2 \cos(\Omega(\tau_1 - \tau_2)) + \cos(\Theta(\tau_1 - \tau_2))$$

$$+ 8 \cos\left(\frac{\Omega}{2}(\tau_1 - \tau_2)\right) \left(\cos\left(\frac{\mathcal{D}_1}{2}(\tau_1 + \tau_2)\right) \cos(2\xi) \sin\left(\frac{\Theta}{2}(\tau_1 - \tau_2)\right) \right)$$

$$- \sin\left(\frac{\mathcal{D}_1}{2}(\tau_1 + \tau_2)\right) \cos\left(\frac{\Theta}{2}(\tau_1 - \tau_2)\right) \right)$$

$$= \frac{1}{8} \left(1 + \sin^2\left(\frac{\Theta}{2}(\tau_1 - \tau_2)\right) \cos(4\xi) + 2\cos^2\left(\frac{\Omega}{2}(\tau_1 - \tau_2)\right) + \cos^2\left(\frac{\Theta}{2}(\tau_1 - \tau_2)\right) \right)$$

$$+ 4\cos\left(\frac{\Omega}{2}(\tau_1 - \tau_2)\right) \left(\cos\left(\frac{\mathcal{D}_1}{2}(\tau_1 + \tau_2)\right) \cos(2\xi) \sin\left(\frac{\Theta}{2}(\tau_1 - \tau_2)\right) \right)$$

$$- \sin\left(\frac{\mathcal{D}_1}{2}(\tau_1 + \tau_2)\right) \cos\left(\frac{\Theta}{2}(\tau_1 - \tau_2)\right) \right) \right)$$
(C18)

When $\mathcal{D}_2 = 0$, the fidelity reduces to the form in \mathcal{F}_{3P} . When $\tau_1 = \tau_2 = \tau/2$:

$$\mathcal{F}_{5P} = \frac{1}{2} - \frac{1}{2} \sin\left(\frac{\mathcal{D}_1}{2}\tau\right) \tag{C19}$$

In this form, $\mathcal{F}_{5P} = 1$ when $\tau = \pi/\mathcal{D}_1 + 2\pi k/\mathcal{D}_1$ for $k \in \mathbb{Z}$, as expected.

Appendix D: Upper Bound to the Fidelity Value

To compute fidelity, we will use Eq. 20:

$$\mathcal{F} = \langle \Psi | \, \hat{\rho}(t) \, | \Psi \rangle \tag{D1}$$

Where $\hat{\rho}(t)$ is the density matrix after spin evolution that includes spin-spin relaxation effects, and

$$|\Psi\rangle = \hat{U}_{CNOT} |S\rangle \tag{D2}$$

This equation will be used because, due to relaxation, $\operatorname{Tr} \hat{\rho}(t) \neq 1$. The main difference between these derivations and ones without relaxation effects is that spin evolution has to be done in the Liouville space, by:

$$\hat{\hat{\rho}}(t+\delta t) = \exp\left[-\left(i\hat{\hat{H}} + \hat{\hat{K}}\right)\delta t\right]\hat{\hat{\rho}}(t) \tag{D3}$$

Where $\hat{\hat{\rho}}(t)$ is a vectorised density matrix, $\hat{\hat{H}}$ is the Hamiltonian superoperator,

$$\hat{\hat{H}} = \hat{H} \otimes \mathbb{I}_d - \mathbb{I}_d \otimes \hat{H}^T, \tag{D4}$$

and \hat{K} is the relaxation superoperator for spin-spin (T_2) relaxation:⁶¹

Here T_2 is spin-spin relaxation lifetime and diag(·) is a diagonal matrix. We assume that T_2 relaxation lifetimes are equal for both sites, that there are no cross-relaxation events, and that spin-lattice relaxation lifetime T_1 is much longer than T_2 and is negligible in the dynamics.

Ideal pulses do not involve spin evolution (they are approximated as being instantaneous) and can be carried out in Hilbert space.

1. Three Pulse Sequence

The \mathcal{F}_{3P} for the pulse sequence in Eq. 56 with T_2 relaxation:

$$\mathcal{F}_{3P} = \langle S | \hat{U}_{CNOT}^{\dagger} \sigma \hat{U}_{CNOT} | S \rangle$$

$$= \frac{1}{4} \left(1 + \frac{1}{2} \cos \left(\Omega(\tau_1 - \tau_2) \right) + \frac{1}{2} \cos \left(\Delta \omega(\tau_1 - \tau_2) \right) + 2e^{-\frac{(\tau_1 + \tau_2)}{T_2}} \sin \left(\frac{\mathcal{D}_1}{2} (\tau_1 + \tau_2) \right) \cos \left(\frac{\Omega}{2} (\tau_1 - \tau_2) \right) \cos \left(\frac{\Delta \omega}{2} (\tau_1 - \tau_2) \right) \right)$$
(D6)

When $T_2 \to \infty$, we get the right form without relaxation effects. Moreover, \mathcal{F}_{3P} is largest when:

$$\begin{cases}
\cos\left(\Omega(\tau_1 - \tau_2)\right) = 1 \\
\cos\left(\Delta\omega(\tau_1 - \tau_2)\right) = 1 \\
\sin\left(\frac{\mathcal{D}_1}{2}(\tau_1 + \tau_2)\right)\cos\left(\frac{\Omega}{2}(\tau_1 - \tau_2)\right)\cos\left(\frac{\Delta\omega}{2}(\tau_1 - \tau_2)\right) = 1
\end{cases} \tag{D7}$$

An upper bound to \mathcal{F}_{3P} naturally emerges for total gate time τ (τ can also include the time it would normally take pulse sequences to act to get the ideal pulses sequence values, so it can be extended to total gate time in a real experiment):

$$\frac{1}{2} + \frac{1}{2}e^{-\frac{\tau_1 + \tau_2}{T_2}} = \frac{1}{2} + \frac{1}{2}e^{-\frac{\tau}{T_2}} \ge \mathcal{F}_{3P}(\tau, \Omega, \Delta\omega, \mathcal{D}_1, T_2)$$
 (D8)

Here $\tau = \tau_1 + \tau_2$.

2. Five Pulse Sequence

The \mathcal{F}_{5P} for the pulse sequence in Eq. 58 with T_2 relaxation:

$$\mathcal{F}_{5P} = \langle S | \hat{U}_{CNOT}^{\dagger} \sigma \hat{U}_{CNOT} | S \rangle$$

$$= \frac{1}{8} \left(1 + \sin^2 \left(\frac{\Theta}{2} (\tau_1 - \tau_2) \right) \cos(4\xi) + 2 \cos^2 \left(\frac{\Omega}{2} (\tau_1 - \tau_2) \right) + \cos^2 \left(\frac{\Theta}{2} (\tau_1 - \tau_2) \right) \right)$$

$$+ 4e^{-\frac{\tau_1 + \tau_2}{T_2}} \cos \left(\frac{\Omega}{2} (\tau_1 - \tau_2) \right) \left(\cos \left(\frac{\mathcal{D}_1}{2} (\tau_1 + \tau_2) \right) \cos(2\xi) \sin \left(\frac{\Theta}{2} (\tau_1 - \tau_2) \right) \right)$$

$$- \sin \left(\frac{\mathcal{D}_1}{2} (\tau_1 + \tau_2) \right) \cos \left(\frac{\Theta}{2} (\tau_1 - \tau_2) \right) \right)$$
(D9)

When $T_2 \to \infty$ we get the right form without relaxation effects. Moreover, \mathcal{F}_{5P} is largest with the same conditions as \mathcal{F}_{3P} and we get identical upper bound for total gate time τ :

$$\frac{1}{2} + \frac{1}{2}e^{-\frac{\tau}{T_2}} \ge \mathcal{F}_{5P}\left(\tau, \Omega, \Delta\omega, \mathcal{D}_1, \mathcal{D}_2, T_2\right) \tag{D10}$$

REFERENCES

¹M. R. Wasielewski, M. D. E. Forbes, N. L. Frank, K. Kowalski, G. D. Scholes, J. Yuen-Zhou, M. A. Baldo, D. E. Freedman, R. H. Goldsmith, T. Goodson, M. L. Kirk, J. K. McCusker, J. P. Ogilvie, D. A. Shultz, S. Stoll, and K. B. Whaley, "Exploiting chemistry and molecular systems for quantum information science," Nature Reviews Chemistry 4, 490–504 (2020).

- ²J. N. Nelson, J. Zhang, J. Zhou, B. K. Rugg, M. D. Krzyaniak, and M. R. Wasielewski, "Cnot gate operation on a photogenerated molecular electron spin-qubit pair," The Journal of Chemical Physics **152**, 014503 (2020).
- ³B. K. Rugg, M. D. Krzyaniak, B. T. Phelan, M. Ratner, R. M. Young, and M. R. Wasielewski, "Photodriven quantum teleportation of an electron spin state in a covalent donor–acceptor–radical system," Nature chemistry **11**, 981–986 (2019).
- ⁴B. W. Stein, C. R. Tichnell, J. Chen, D. A. Shultz, and M. L. Kirk, "Excited state magnetic exchange interactions enable large spin polarization effects," Journal of the American Chemical Society **140**, 2221–2228 (2018).
- ⁵M. M. Paquette, D. Plaul, A. Kurimoto, B. O. Patrick, and M. L. Frank, "Opto-spintronics: photoisomerization-induced spin state switching at 300 k in photochrome cobalt–dioxolene thin films," Journal of the American Chemical Society **140**, 14990–15000 (2018).
- ⁶M. Atzori and R. Sessoli, "The second quantum revolution: role and challenges of molecular chemistry," Journal of the American Chemical Society **141**, 11339–11352 (2019).
- ⁷L. V. H. Rodgers, L. B. Hughes, M. Xie, P. Maurer, S. Kolkowitz, A. Jayich, and N. P. De Leon, "Materials challenges for quantum technologies based on color centers in diamond," Mrs Bulletin 46, 623–633 (2021).
- ⁸G.-Q. Liu and X.-Y. Pan, "Quantum information processing with nitrogenvacancy centers in diamond," Chinese Physics B **27**, 020304 (2018).
- ⁹R. J. Epstein, F. M. Mendoza, Y. K. Kato, and D. D. Awschalom, "Anisotropic interactions of a single spin and dark-spin spectroscopy in diamond," Nature Physics **1**, 94–98 (2005).
- ¹⁰X. Rong, J. Geng, F. Shi, Y. Liu, K. Xu, W. Ma, F. Kong, Z. Jiang, Y. C. Wu, and J. Du, "Experimental fault-tolerant universal quantum gates with solid-state spins under ambient conditions," Nature Communications 6 (2015), 10.1038/ncomms9748.
- ¹¹D. D. Sukachev, A. Sipahigil, C. N. Nguyen, M. K. Bhaskar, R. J. Evans, F. Jelezko, and M. D. Lukin, "Silicon-Vacancy Spin Qubit in Diamond: A Quantum Memory Exceeding 10 ms with Single-Shot State Readout," Physical Review Letters 119 (2017), 10.1103/physrevlett.119.223602.
- ¹²B. C. Rose, D. Huang, Z.-H. Zhang, P. J. Stevenson, A. M. Tyryshkin, S. Sangtawesin, S. Srinivasan, L. Loudin, M. Markham, A. Edmonds, D. J. Twitchen, S. A. Lyon, and N. P. De Leon, "Observation of an environmentally insensitive solid-state spin defect in diamond," Science 361, 60–63 (2018).

- ¹³J. C. McCallum, B. M. Johnson, and T. Botzem, "Donor-based qubits for quantum computing in silicon," Applied physics reviews **8**, 031314 (2021).
- ¹⁴J. T. O'Brien, S. R. Schofield, M. Y. Simmons, R. M. Clark, A. S. Dzurak, N. J. Curson, B. E. Kane, N. McAlpine, M. E. Hawley, and G. V. Brown, "Towards the fabrication of phosphorus qubits for a silicon quantum computer," Physical review 64 (2001), 10.1103/physrevb.64.161401.
- ¹⁵X. Mi, M. Benito, S. Putz, D. M. Zajac, J. M. Taylor, G. Burkard, and J. R. Petta, "A coherent spinphoton interface in silicon," Nature 555, 599–603 (2018).
- ¹⁶M. A. Eriksson, M. Friesen, S. Coppersmith, R. Joynt, L. Klein, K. A. Slinker, C. Tahan, P. M. Mooney, J. Chu, and S. J. Koester, "Spin-Based Quantum Dot Quantum Computing in Silicon," Quantum Information Processing 3, 133–146 (2004).
- ¹⁷Q. Li, Cywiski, D. Culcer, X. Hu, and S. D. Sarma, "Exchange coupling in silicon quantum dots: Theoretical considerations for quantum computation," Physical Review B 81 (2010), 10.1103/physrevb.81.085313.
- ¹⁸K. Wang, G. Xu, F. Gao, H. Liu, R.-L. Ma, X. Zhang, Z. Wang, G. Cao, T. Wang, J. Zhang, D. Culcer, X. Hu, H.-W. Jiang, H.-O. Li, G.-C. Guo, and G.-C. Guo, "Ultrafast coherent control of a hole spin qubit in a germanium quantum dot," Nature Communications 13 (2022), 10.1038/s41467-021-27880-7.
- ¹⁹C. Kloeffel and D. Loss, "Prospects for Spin-Based Quantum Computing in Quantum Dots," Annual Review of Condensed Matter Physics 4, 51–81 (2013).
- ²⁰G. Scappucci, C. Kloeffel, F. A. Zwanenburg, D. Loss, M. Myronov, J. Zhang, S. De Franceschi, G. Katsaros, and M. Veldhorst, "The germanium quantum information route," Nature Reviews Materials 6, 926–943 (2020).
- ²¹C. D. Buckley, D. A. Hunter, P. J. Hore, and K. A. McLauchlan, "Electron spin resonance of spin-correlated radical pairs," Chemical Physics Letters **135**, 307–312 (1987).
- ²²W. Lubitz, F. Lendzian, and R. Bittl, "Radicals, radical pairs and triplet states in photosynthesis," Accounts of chemical research **35**, 313–320 (2002).
- ²³T. P. Fay, L. P. Lindoy, and D. E. Manolopoulos, "Spin-selective electron transfer reactions of radical pairs: Beyond the haberkorn master equation," The Journal of Chemical Physics 149, 064107 (2018).
- ²⁴A. M. Lewis, T. P. Fay, D. E. Manolopoulos, C. Kerpal, S. Richert, and C. R. Timmel, "On the low magnetic field effect in radical pair reactions," The Journal of Chemical Physics

- **149**, 034103 (2018).
- ²⁵T. P. Fay, A. M. Lewis, and D. E. Manolopoulos, "Spin-dependent charge recombination along para-phenylene molecular wires," The Journal of Chemical Physics 147, 064107 (2017).
- ²⁶D. P. DiVincenzo, "The physical implementation of quantum computation," Fortschritte der Physik: Progress of Physics 48, 771–783 (2000).
- ²⁷M.Y.Volkov and K.M.Salikhov, "Pulse protocols for quantum computing with electron spins as qubits," Appl. Magn. Reson. **41**, 145–154 (2011).
- ²⁸U. E. Steiner and U. Thomas, "Magnetic field effects in chemical kinetics and related phenomena," Chemical Reviews **89**, 51–147 (1989).
- ²⁹K. McLauchlan and U. Steiner, "The spin-correlated radical pair as a reaction intermediate," Molecular Physics **73**, 241–263 (1991).
- ³⁰J. A. Weil and J. R. Bolton, <u>Electron Paramagnetic Resonance</u>: <u>Elementary Theory and Practical Application</u> 2nd ed. (John Wiley & Sons, 2007).
- ³¹Y. Zhang, C.A.Ryan, R. Laflamme, and J. Baugh, "Coherent control of two nuclear spins using the anisotropic hyperfine interaction," Phys. Rev. Lett. **107**, 170503 (2011).
- ³²J. Tang and J. Norris, "Multiple-quantum epr coherence in a spin-correlated radical pair system," Chemical Physics Letters **233**, 192–200 (1995).
- ³³J. Tang, M. C. Thurnauer, and J. R. Norris, "Electron spin echo envelope modulation due to exchange and dipolar interactions in a spin-correlated radical pair," Chemical Physics Letters 219, 283–0290 (1994).
- $^{34}\,\mathrm{``Epr}$ of spin-correlated radical pairs, analytical treatment of selective excitation including zero-quantum coherence," .
- ³⁵M. Price, S. S. Somaroo, C. Tseng, J. C. Gore, A. Fahmy, T. Havel, and D. Cory, "Construction and implementation of nmr quantum logic gates for two spin systems," Journal of Magnetic Resonance 140, 371–378 (1999).
- ³⁶M. Nielsen and I. Chuang, <u>Quantum computation and quantum information</u> (American Association of Physics Teachers, 2002).
- ³⁷J. N. Nelson, J. Zhang, J. Zhou, B. K. Rugg, M. D. Krzyaniak, and M. R. Wasielewski, "Cnot gate operation on a photogenerated molecular electron spin-qubit pair," The Journal of Chemical Physics, 014503 (2020).
- ³⁸J. N. Nelson, J. Zhang, J. Zhou, B. K. Rugg, M. D. Krzyaniak, and M. R. Wasielewski,

- "Effect of electron–nuclear hyperfine interactions on multiple-quantum coherences in photogenerated covalent radical (qubit) pairs," The Journal of Physical Chemistry A 122, 9392–9402 (2018).
- ³⁹J. N. Nelson, M. D.Krzyaniak, N. E. Horwitz, B. K. Rugg, B. T. Phelan, and M. R. Wasielewski, "Zero quantum coherence in a series of covalent spin-correlated radical pairs," The Journal of Physical Chemistry A 121, 2241–2252 (2017).
- ⁴⁰S. M. Harvey and M. R. Wasielewski, "Photogenerated spin-correlated radical pairs: From photosynthetic energy transduction to quantum information science," Journal of the American Chemical Society **143**, 15508–15529 (2021).
- ⁴¹R. Carmieli, Q. Mi, A. N. Ricks, E. M. Giacobbe, S. M. Mickley, and M. R. Wasielewski, "Direct measurement of photoinduced charge separation distances in donor- acceptor systems for artificial photosynthesis using oop-eseem," Journal of the American Chemical Society **131**, 8372–8373 (2009).
- ⁴²A. D. Becke, "Beckes three parameter hybrid method using the lyp correlation functional," J. Chem. Phys, volume=.
- ⁴³P. J. Stephens, F. J. Devlin, C. F. Chabalowski, and M. J. Frisch, "Ab initio calculation of vibrational absorption and circular dichroism spectra using density functional force fields," The Journal of Physical Chemistry 98, 11623–11627 (1994).
- ⁴⁴F. Weigend and R. Ahlrichs, "Balanced basis sets of split valence, triple zeta valence and quadruple zeta valence quality for h to rn: Design and assessment of accuracy," Physical Chemistry Chemical Physics **7**, 3297–3305 (2005).
- ⁴⁵F. Weigend, "Accurate coulomb-fitting basis sets for h to rn," Physical Chemistry Chemical Physics 8, 1057–1065 (2006).
- ⁴⁶S. Grimme, "Semiempirical gga-type density functional constructed with a long-range dispersion correction," Journal of Computational Chemistry **27**, 1787–1799 (2006).
- ⁴⁷S. Grimme, J. Antony, S. Ehrlich, and H. Krieg, "A consistent and accurate ab initio parametrization of density functional dispersion correction (dft-d) for the 94 elements h-pu," The Journal of chemical physics **132**, 154104 (2010).
- ⁴⁸S. Grimme, S. Ehrlich, and L. Goerigk, "Effect of the damping function in dispersion corrected density functional theory," Journal of Computational Chemistry **32**, 1456–1465 (2011).
- $^{49}\mathrm{A.~D.~Becke,~"Density-functional~exchange-energy~approximation~with~correct~asymptotic}$

- behavior," Physical review A 38, 3098 (1988).
- ⁵⁰N. Rega, M. Cossi, and V. Barone, "Development and validation of reliable quantum mechanical approaches for the study of free radicals in solution," The Journal of chemical physics **105**, 11060–11067 (1996).
- ⁵¹T. H. Dunning, "Gaussian basis sets for use in correlated molecular calculations. i. the atoms boron through neon and hydrogen," The Journal of Chemical Physics **90**, 1007–1023 (1989).
- ⁵²D. E. Woon and T. H. Dunning, "Calculation of the electron affinities of the second row atoms: Al–cl," The Journal of Chemical Physics **99**, 3730–3737 (1993).
- ⁵³F. Neese, "The orca program system," Wiley Interdisciplinary Reviews: Computational Molecular Science 2.
- ⁵⁴F. Neese, "Software update: the orca program system, version 4.0," Wiley Interdisciplinary Reviews-Computational Molecular Science 8, 73–78 (2017).
- ⁵⁵T. P. Fay, A. M. Lewis, and D. E. Manolopoulos, "Spin-dependent charge recombination along para-phenylene molecular wires," The Journal of Chemical Physics 147, 064107 (2017).
- ⁵⁶K. Schulten and P. G. Wolynes, "Semiclassical description of electron spin motion in radicals including the effect of electron hopping," The Journal of Chemical Physics **68**, 3292–3297 (1978).
- ⁵⁷P. de Fouquieres, S. G. Schirmer, S. J. Glaser, and I. Kuprov, "Second order gradient ascent pulse engineering," Journal of Magnetic Resonance **212**, 412–417 (2011).
- ⁵⁸B. Rowland and J. A. Jones, "Implementing quantum logic gates with gradient ascent pulse engineering: principles and practicalities," Philosophical Transactions of the Royal Society A: Mathematical, Physical and Engineering Sciences **370**, 4636–4650 (2012).
- ⁵⁹N. N. Khaneja, T. Reiss, C. Kehlet, T. Schulte-Herbrüggen, and S. J. Glaser, "Optimal control of coupled spin dynamics: design of nmr pulse sequences by gradient ascent algorithms," Journal of Magnetic Resonance **172**, 296–305 (2005).
- ⁶⁰J. Jones, R. Hansen, and M. Mosca, "Quantum logic gates and nuclear magnetic resonance pulse sequences," Journal of Magnetic Resonance 135, 353–360 (1998).
- ⁶¹S. Macura, Y. Huang, D. Suter, and R. Ernst, "Two-dimensional chemical exchange and cross-relaxation spectroscopy of coupled nuclear spins," Journal of Magnetic Resonance (1969) **43**, 259–281 (1981).